PERGAMON

International Journal of Multiphase Flow 26 (2000) 783–831

International Journal of Multiphase Flow

www.elsevier.com/locate/ijmulflow

# Flow of spatially non-uniform suspensions. Part I: Phenomenology

M. Marchioro, M. Tanksley, A. Prosperetti*, [1]

*Department of Mechanical Engineering, The Johns Hopkins University, Baltimore, MD 21218, USA*

Received 19 August 1998; received in revised form 1 June 1999

**Abstract**

The response of a spatially non-uniform suspension of spheres to several forcing agents — forces and torques applied to the spheres, and an imposed simple shear — is studied numerically for Stokes flow conditions. While the standard results are recovered in the uniform case, it is found that the non-uniformity of the particle probability distribution gives rise to qualitatively new features. For example, the rheological behavior of the system cannot be described solely in terms of an effective viscosity; a relative velocity between particles and fluid can arise; the particles can either lead or lag the local angular velocity of the fluid elements. It is shown that a mixture effective viscosity can be calculated for all three cases with mutually consistent results. In a subsequent paper the present results will be used to derive in a systematic way closure relations for an averaged-equations description of the suspension. 

*Keywords:* Suspensions; Spatial non-uniformity; Direct numerical simulation

## 1. Introduction

The central difficulty in the derivation of averaged equations for disperse multiphase flow is the so called closure problem: any form of averaging leads to more unknowns than the available equations and, therefore, some of the information lost in the averaging process must

* Corresponding author. Tel.: +1-410-516-8534; fax: +1-410-516-7254.

*E-mail address:* prosperetti@jhu.edu (A. Prosperetti).

[1] Also, Faculty of Applied Physics and Twente Institute of Mechanics, University of Twente, AE 7500 Enschede, The Netherlands, and Burgerscentrum, The Netherlands.

0301-9322/00/$ - see front matter 
PII: S0301-9322(99)00068-3

be reintroduced. No systematic way of achieving this objective has been devised save for a few simple and highly restricted cases such as spatially periodic systems (see e.g. Hasimoto, 1959; Sangani and Acrivos, 1982, 1983; Zuzovsky et al., 1983; Nunan and Keller, 1984; Sangani and Yao, 1988) or dilute suspensions (see e.g. Batchelor, 1972; Hinch, 1977; Acrivos et al., 1980; Biesheuvel and Spoelstra, 1989).[2] Aside from a handful of notable exceptions (Feuillebois, 1984; Lhuillier, 1992; Lhuillier and Nozières, 1992; Buyevich, 1995; Buyevich and Ustinov, 1995), a fundamental restriction in all previous studies on this topic is the assumption of spatial uniformity of the system. While this assumption may be useful when the macroscopic length scale is much larger than the particle scale, there are situations where it is clearly insufficient such as in the transition region between the clear fluid and the suspension, when particles accumulate in certain flow structures such as vortices and wall layers, and others. But, more importantly, spatial uniformity eliminates many, if not all, terms containing derivatives and therefore has a profound effect on the mathematical structure of the resulting equations. The very familiar problem of lack of hyperbolicity of most averaged equations models (see e.g. Stewart and Wendroff, 1984; Jones and Prosperetti, 1985) stems from the uncertainties clouding the proper formulation of these differential terms.

In the present paper and its sequel (Marchioro et al., 2000, hereafter referred to as Part II) we describe a method by which the direct numerical simulation of some prototypical physical problems, in combination with an effective form of averaging, may be used to help find the correct closure relations. While we confine ourselves to the case of Stokes flow at the particle scale, the method that we describe has a wider applicability, e.g. to potential flow and heat conduction (Marchioro and Prosperetti, 1999). Furthermore, Stokes flow at the local scale does not imply Stokes flow on the global macroscopic scale (see e.g. Feuillebois, 1984), and therefore the constitutive relations that we derive in Part II are applicable to a rather broad range of phenomena.

The results obtained in this paper are a necessary step for the derivation of those presented in Part II, but are also of interest in themselves as they illustrate the many *qualitatively novel* aspects in which a non-uniform suspension differs from a uniform one. Examples are a proof of the non-Newtonian nature of the mixture stress, a non-zero inter-phase slip velocity in simple shear flow, and the appearance of mean vorticity in sedimentation. In Part II, we shall introduce in a systematic way constitutive relations that are capable of accounting for these aspects of suspension behavior.

In addressing the problem of non-uniform suspensions one faces the difficulty that most of the usual approaches are either severely limited (e.g., to the dilute case) or downright inadequate (e.g., those that appeal to physical intuition mostly based on the behavior of one or two particles). Nonuniformity is an issue precisely because its effects are difficult to anticipate by physical intuition. Numerical methods are, therefore, necessary to deal with the problem. Several approaches to simulate general flows at both zero (see e.g. Brady and Bossis, 1988; Weinbaum et al., 1990; Cichocki et al., 1994; Nott and Brady, 1994; Chang and Powell, 1994a, 1994b; Sangani et al., 1996; Ladd, 1997) and finite (see e.g. Unverdi and Tryggvason, 1992;

[2] The literature on the subject is quite extensive and we limit ourselves to a few representative papers. Furthermore, no references are given to the large literature based on more or less ad hoc approximations.

Feng et al., 1994; Tezduyar and Mittal, 1994; Johnson and Tezduyar, 1996, 1997; Kaftori et al., 1995a, 1995b; Pan and Banerjee, 1996; Hu, 1996; Esmaeeli and Tryggvason, 1996) Reynolds numbers are available, but they are not suitable to isolate specifically the effects of spatial non-uniformities as their effectiveness — almost by definition — consists in their ability to account simultaneously for the entire multi-faceted complexity of the flow. For our purposes the most promising techniques are those developed for infinitely extended, spatially uniform mixtures (see e.g. Mo and Sangani, 1994, 1996; Ladd, 1988, 1990, 1993). In this paper, we describe a method that extends these powerful procedures to the non-uniform case.

At present our simulation program is somewhat limited by the available computational resources and, therefore, the numerical results that we present are not as accurate as it would be desirable. Nevertheless, the methods that we describe are of general validity and ready to be used to refine the present results when better hardware and software will become available.

The present study is based on the completely random hard-sphere probability distribution well known e.g. in the theory of the liquid state (see e.g. Allen and Tildesley, 1987; Hansen and McDonald, 1990; Balucani and Zoppi, 1994). This probability distribution is not entirely realistic for a flowing suspension (see e.g. Batchelor and Green, 1972; Zuzovsky et al., 1983; Brady and Morris, 1997). Nevertheless, we believe that the present results are interesting for a number of reasons. In the first place, these are the first results to show the difference between homogeneous and non-homogeneous suspensions. As such, they are of considerable interest in themselves. It may be expected that, qualitatively, many of our conclusions would hold irrespective of the type and magnitude of non-uniformity. Secondly, as will be shown in Part II of this study, our method will make it possible to systematically derive closure relations for the averaged equations the functional form of which, again, may be expected to be relatively robust with respect to the underlying probability distribution. A more realistic probability distribution will undoubtedly change the value of the closure coefficients (e.g., the effective viscosity), but would not be expected to drastically alter the structure of the closure relations. Thirdly, these are the first results to show that the effective viscosity of a random suspension is a robust flow property, that has the same numerical value for a number of different flow situations.

## 2. Some considerations on numerical simulation methods

A significant fraction of the literature on suspensions or, more generally, composites, attempts to characterize their behavior in terms of effective properties such as mixture viscosity (see e.g. Batchelor, 1970; Batchelor and Green, 1972; Nunan and Keller, 1984; Martys et al., 1994) or effective thermal conductivity (see e.g. Jeffrey, 1973; Sangani and Acrivos, 1983; Torquato, 1987; Sangani and Yao, 1988; Bonnecaze and Brady, 1991; Buyevich and Ustinov, 1995). Although the terms that describe these effects ultimately appear in the averaged equations in a differential form, such effective properties may be calculated by assuming a spatially uniform particle distribution using techniques similar to those developed in the kinetic theory of gases (see e.g. Chapman and Cowling, 1952; Landau and Lifshitz, 1969; Cercignani, 1988).

A powerful numerical technique is available to deal with such situations: an infinite uniform

suspension is approximated by the periodic repetition of a fundamental cell in which particles are randomly distributed. Numerically, this amounts to carrying out the simulation in a finite box with periodic boundary conditions (see e.g. Sangani and Yao, 1988; Mo and Sangani, 1994, 1996; Ladd, 1988, 1990, 1993). While powerful, this approach can only work for a subset of special terms that enter the averaged equations as the divergences of suitable fluxes. As will be seen later, and in particular in Part II, not all the required differential terms have this nature.

As mentioned in the previous section, other methods exists for the simulation of (relatively simple) actual flows. Of course, non-zero gradients — e.g. in the velocity field — exist in such flows, but their usefulness for the specific purpose of developing closure relations is somewhat limited. The typical approach is to postulate closure relations and to show that solutions of the averaged equations thus generated match the averages of the direct numerical simulation results (see e.g. Nott and Brady, 1994). While of course useful, such an approach is, first of all, not systematic and, secondly, it has to rely on the effects of spatial non-uniformities to be large enough to emerge above the statistical noise of the simulations. Thus, some effects may be missed because their magnitude happened to be small in the particular situation simulated. Thirdly, in an actual flow, gradients are seldom spatially uniform and this complicates even further the identification of their effects. While not completely immune from these limitations, the method that will be described below appears to represent an improvement or, at least, a useful complement to this class of numerical simulation techniques.

A rather straightforward way to extend the periodic cell method previously mentioned to deal, for example, with a non-uniform spatial distribution of the disperse phase would be to retain the spatial periodicity in two directions but to give it up in the third one. One could stack many planes, each containing two-dimensional cells, at different distances from each other so as to generate a spatial gradient in the direction normal to the planes. Such an approach is feasible, but it is severely limited by the large increase in computational cost, the presence of 'end effects' of uncertain magnitude and, more importantly, by the fact that the maximum gradient achievable in practice, while still satisfying the separation of micro- and macro-scale constraint, is so small as to render problematic the unambiguous determination of its effects.

These considerations point to the necessity of a new approach to the problem that we describe in Section 5 after a brief exposition of the averaging techniques (Section 3), and their application to the momentum equation (Section 4). In Section 6, we develop a form of the averaged fields in terms of quantities that are calculated numerically in Sections 8–10. Some details on the computations are given in Section 7.

## 3. Averaging

Some of the average quantities of interest, such as the mean particle velocity, are very directly related to the corresponding microscopic variables and can readily be obtained from the results of the numerical simulations. Other average quantities, however, are intrinsically macroscopic constructs that have no direct counterpart at the microscopic level. A typical example is the mixture stress which does not exist at the microscopic level, while it plays an

essential role at the macroscopic one. Such purely macroscopic quantities are the result of averaging procedures applied to the microscopic equations. Their explicit expression in terms of microscopic variables, which is evidently needed to compute them, necessarily requires therefore the explicit use of a specific averaging procedure. Here, we use an ensemble-based phase averaging method that has been developed specifically for this purpose. A detailed description is given in our earlier papers (Zhang and Prosperetti, 1994a, 1994b, 1997; Prosperetti, 1998). Here, we only provide a few basic relations to which it will be necessary to refer below.

In the absence of inertial effects, for $N$ equal homogeneous spherical particles, the flow is uniquely determined once the configuration $\mathscr{C}^N$ — i.e., the position of the centers $\mathbf{y}^\alpha$, $\alpha = 1,2,\ldots,N$ of the $N$ particles — is given. The probability density of the configuration $\mathscr{C}^N$ is denoted by $P(N)$.

In terms of the characteristic functions $\chi_{C,D}(\mathbf{x};N)$ for the continuous (subscript $C$) or disperse (subscript $D$) phases, the phase ensemble average of the generic quantity $f_{C,D}$ pertaining to either phase is defined by

$$\beta_{C,D} f_{C,D} = \frac{1}{N!}\int \mathrm{d}\mathscr{C}^N\, P(N)\chi_{C,D}(\mathbf{x};N) f_{C,D}(\mathbf{x};N), \tag{1}$$

where $\beta_{C,D}$ are the volume fractions defined by this same equation with $f_{C,D} = 1$. Here and in the following the explicit indication of time dependence is suppressed. Since the particle-fluid interfaces have zero measure

$$\beta_C + \beta_D = 1. \tag{2}$$

For a generic quantity $g^{(\alpha)}$ pertaining to the $\alpha$th particle as a whole (such as the center-of-mass velocity) we use a *particle average* defined by

$$n(\mathbf{x})\bar{g}(\mathbf{x}) = \frac{1}{N!}\int \mathrm{d}\mathscr{C}^N\, P(N)\left[\sum_{\alpha=1}^{N}\delta\big(\mathbf{x}-\mathbf{y}^{(\alpha)}\big)g^{(\alpha)}(N)\right], \tag{3}$$

where $n$ is the particle number density defined by this same equation with $g^{(\alpha)} = 1$:

$$n(\mathbf{x}) = \frac{1}{N!}\int \mathrm{d}\mathscr{C}^N\, P(N)\left[\sum_{\alpha=1}^{N}\delta\big(\mathbf{x}-\mathbf{y}^{(\alpha)}\big)\right]. \tag{4}$$

If averaged quantities vary slowly over distances comparable to the particle radius, accurate to second order in the ratio $a/L$ of the particle radius to the macroscopic length scale $L$, one has

$$\beta_D = v\left(1+\frac{a^2}{10}\nabla^2\right)n, \tag{5}$$

where $v = \frac{4}{3}\pi a^3$ is the particle volume.

Upon assuming the fluid to be incompressible, averaging of the microscopic equation of continuity leads to

$$\frac{\partial \beta_C}{\partial t} + \nabla \cdot \left(\beta_C \langle \mathbf{u}_c \rangle\right) = 0, \tag{6}$$

and, similarly,

$$\frac{\partial \beta_D}{\partial t} + \nabla \cdot \left(\beta_D \langle \mathbf{u}_D \rangle\right) = 0, \tag{7}$$

where $\mathbf{u}_{C,D}$ are the velocities of the phases. In view of Eq. (2), adding Eqs. (6) and (7) we find

$$\nabla \cdot \mathbf{u}_m = 0, \tag{8}$$

where the mean volumetric flux $\mathbf{u}_m$ is defined by

$$\mathbf{u}_m = \beta_C \langle \mathbf{u}_C \rangle + \beta_D \langle \mathbf{u}_D \rangle. \tag{9}$$

or, from Eq. (1),

$$\mathbf{u}_m = \frac{1}{N!} \int \mathrm{d}\mathscr{C}^N \, P(N) \left[\chi_C(\mathbf{x};N)\mathbf{u}_C(\mathbf{x};N) + \chi_D(\mathbf{x};N)\mathbf{u}_D(\mathbf{x};N)\right]. \tag{10}$$

Expressing the conservation of particle number

$$\frac{\partial n}{\partial t} + \nabla \cdot (n\bar{\mathbf{w}}) = 0, \tag{11}$$

requires the velocity field $\bar{\mathbf{w}}$ which is defined as the particle average (3) of the center-of-mass velocity of the particles $\mathbf{w}^\alpha$. In general, $\bar{\mathbf{w}} \neq \langle \mathbf{u}_D \rangle$ but, analogously to Eq. (5), it can be shown that, accurate to second order in the ratio $a/L$,[3]

$$\beta_D \langle \mathbf{u}_D \rangle = \left(1 + \frac{a^2}{10}\nabla^2 + \frac{a^4}{280}\nabla^4\right)(nv\bar{\mathbf{w}}) + \frac{a^2}{5}\left(1 + \frac{a^2}{14}\nabla^2\right)\nabla \times (nv\bar{\boldsymbol{\Omega}}) \tag{12}$$

where $\bar{\boldsymbol{\Omega}}$ is the particle-average angular velocity.

## 4. Averaged momentum equations

Upon incorporating the body force into a modified pressure, the Stokes equations for the continuous phase may be written as

$$\nabla \cdot \boldsymbol{\sigma}_C = 0, \tag{13}$$

where the stress $\boldsymbol{\sigma}_C$ is given by

$$\boldsymbol{\sigma}_C = -p_C \mathbf{I} + 2\mu_C \mathbf{e}_C, \tag{14}$$

[3] In some of the problems to be considered here $\bar{\mathbf{w}}$ is found to increase proportionally to $L^2$, and this circumstance reduces the accuracy of this equation from fourth to second order.

in terms of the (modified) pressure $p_C$, identity two-tensor $\mathbf{I}$, viscosity $\mu_C$, and rate of deformation tensor $\mathbf{e}_C$. It is shown in Zhang and Prosperetti (1997) that, since $\mathbf{e}_D$ vanishes for rigid spheres, the ensemble average of $\mathbf{e}_C$ is exactly

$$\langle \mathbf{e}_C \rangle = \frac{1}{\beta_C} \mathbf{E}_m \tag{15}$$

where

$$\mathbf{E}_m = \frac{1}{2}\left[\nabla \mathbf{u}_m + (\nabla \mathbf{u}_m)^{\mathrm{T}}\right] \tag{16}$$

is the rate of deformation tensor based on the mean volumetric flux (9). With this result, the average continuous-phase stress is therefore

$$\beta_C \langle \boldsymbol{\sigma}_C \rangle = -\beta_C \langle p_C \rangle \mathbf{I} + 2\mu_C \mathbf{E}_m. \tag{17}$$

Because of the finite extent of the particles, averaging and differentiation do not commute. However, when the particles are small in comparison with the macroscopic length so that $a/L \ll 1$, one has (Zhang and Prosperetti, 1994a, 1997; Prosperetti, 1998)

$$\nabla \cdot \left(\beta_C \langle \boldsymbol{\sigma}_C \rangle\right) = \beta_C \langle \nabla \cdot \boldsymbol{\sigma}_C \rangle + n\mathscr{A}[\boldsymbol{\sigma}_C] - \nabla \cdot \left(\beta_D \mathscr{L}[\boldsymbol{\sigma}_C]\right), \tag{18}$$

where, approximately,

$$\beta_D \mathscr{L}[\boldsymbol{\sigma}_C] = n\mathscr{T}[\boldsymbol{\sigma}_C] + \nabla \cdot \left\{ n\mathscr{S}[\boldsymbol{\sigma}_C] + \nabla \cdot \left( n\mathscr{R}[\boldsymbol{\sigma}_C] + \cdots \right) \right\}. \tag{19}$$

The quantities introduced in these equations are most usefully expressed in terms of particle averages as follows:

$$\mathscr{A}[\boldsymbol{\sigma}_C](\mathbf{x}) = \overline{\int_{|\mathbf{r}|=a} \mathrm{d}S_r \, \boldsymbol{\sigma}_C(\mathbf{x}+\mathbf{r}|\mathbf{x}) \cdot \mathbf{n}}, \tag{20}$$

$$\mathscr{T}[\boldsymbol{\sigma}_C](\mathbf{x}) = a\overline{\int_{|\mathbf{r}|=a} \mathrm{d}S_r \, \mathbf{n}\left[\boldsymbol{\sigma}_C(\mathbf{x}+\mathbf{r}|\mathbf{x}) \cdot \mathbf{n}\right]}, \tag{21}$$

$$\mathscr{S}[\boldsymbol{\sigma}_C](\mathbf{x}) = -\frac{1}{2}a^2\overline{\int_{|\mathbf{r}|=a} \mathrm{d}S_r \, \mathbf{nn}\left[\boldsymbol{\sigma}_C(\mathbf{x}+\mathbf{r}|\mathbf{x}) \cdot \mathbf{n}\right]}, \tag{22}$$

$$\mathscr{R}[\boldsymbol{\sigma}_C](\mathbf{x}) = \frac{1}{6}a^3\overline{\int_{|\mathbf{r}|=a} \mathrm{d}S_r \, \mathbf{nnn}\left[\boldsymbol{\sigma}_C(\mathbf{x}+\mathbf{r}|\mathbf{x}) \cdot \mathbf{n}\right]}. \tag{23}$$

These forms are particularly useful for numerical computation as will be seen below. In particular, one recognizes $\mathscr{A}$ as the average hydrodynamic force acting on the particles.

By using Eqs. (17) and (18) in the momentum equation (13), we find the averaged continuous phase momentum equation in the form

$$\nabla\cdot\big(-\beta_C\langle p_C\rangle\mathbf{I}+2\mu_C\mathbf{E}_m+\beta_D\mathscr{L}[\boldsymbol{\sigma}_C]\big)=n\mathscr{A}[\boldsymbol{\sigma}_C]. \tag{24}$$

When inertia is negligible, the mean momentum balance for the particles evidently has the form

$$\overline{\int_{|\mathbf{r}|=a}\mathrm{d}S_r\,\boldsymbol{\sigma}_C(\mathbf{x}+\mathbf{r}|\mathbf{x})\cdot\mathbf{n}}+v(\rho_D-\rho_C)\mathbf{g}=0, \tag{25}$$

where $\rho_{C,D}$ are the phase densities and $\mathbf{g}$ is the acceleration of gravity. Since the integral in this equation is precisely equal to $\mathscr{A}$, this quantity may be eliminated from Eq. (24) with the result

$$\nabla\cdot\big(-\beta_C\langle p_C\rangle\mathbf{I}+2\mu_C\mathbf{E}_m+\beta_D\mathscr{L}[\boldsymbol{\sigma}_C]\big)=-nv(\rho_D-\rho_C)\mathbf{g}. \tag{26}$$

The quantity under the divergence sign in Eq. (26) has the physical meaning of a mixture stress. In a recent paper (Marchioro et al., 1999) we have given a detailed study of this quantity identifying the contribution that is to be considered as the mixture pressure $p_m$ and separating it from the viscous part of the stress. The result of that analysis (based on a study of the transformation properties of the stress tensor under gauge transformations of the microscopic pressure $p_C$) is

$$p_m=\beta_C\langle p_C\rangle+\left(1+\frac{a^2}{10}\nabla^2\right)\big[n(\mathbf{x})v\overline{p^e}\big]+\frac{1}{5}a^2\nabla\cdot\left[n(\mathbf{x})\overline{\int_{|\mathbf{r}|=a}\mathrm{d}S\,(-\mathbf{n})p_C}\right]$$
$$+\frac{1}{14}a^2\nabla\nabla:\left[n\overline{\int_{|\mathbf{r}|=a}\left(\mathbf{nn}-\frac{1}{3}\mathbf{I}\right)p_C}\right], \tag{27}$$

where

$$p^e=\frac{1}{4\pi a^2}\int_{|\mathbf{r}|=a}\mathrm{d}S_r\,p_C\big(\mathbf{y}^\alpha+\mathbf{r};N\big), \tag{28}$$

is the average pressure over the particle surface. For a spatially uniform mixture, using Eq. (5), we see that this result may be written as

$$p_m=\beta_C\langle p_C\rangle+\beta_D\overline{p^e}, \tag{29}$$

which is an expression that has been proposed before (Prosperetti and Jones, 1984). The quantity $\overline{p^e}$ has also been introduced before by several authors (see e.g. Ishii, 1975; Drew, 1983). Eq. (27) generalizes this form to the inhomogeneous case.

The remainder of the mixture stress (i.e. the quantity under the divergence sign in Eq. (26)), after subtraction of $p_m\mathbf{I}$ is to be identified with the viscous mixture stress which we write as $2\mu_C\mathbf{E}_m+\boldsymbol{\Sigma}_P$, where the contribution of the particles is

$$\boldsymbol{\Sigma}_P=\big(p_m-\beta_C\langle p_C\rangle\big)\mathbf{I}+\beta_D\mathscr{L}[\boldsymbol{\sigma}_C]. \tag{30}$$

With the definitions (27) and (30), the momentum equation (26) becomes

$$\nabla \cdot \left( -p_m \mathbf{I} + 2\mu_C \mathbf{E}_m + \boldsymbol{\Sigma}_P \right) = -nv(\rho_D - \rho_C)\mathbf{g}, \tag{31}$$

## 5. Periodic cell model for a non-uniform suspension

To introduce the present technique for the generation of a suitable non-uniform ensemble, it is useful to review first the way in which the periodic cell method is used for the direct numerical simulation of unbounded suspensions (see e.g. Sangani and Yao, 1988; Mo and Sangani, 1994). The central idea is to approximate the suspension by filling the whole space with replicas of a fundamental (e.g. cubic) cell containing $N$ identical spheres randomly distributed according to a uniform probability $P_0$.[4] With this construct, the (microscopic) continuous-phase velocity field can be written in the form

$$\mathbf{u}_C(\mathbf{x};N) = \mathbf{U}_\infty(\mathbf{x}) + \tilde{\mathbf{u}}_C(\mathbf{x};N), \tag{32}$$

where $\mathbf{U}_\infty$, is an imposed deterministic velocity field and $\tilde{\mathbf{u}}_C$ is periodic in the three directions perpendicular to the faces of the fundamental cell. The disperse-phase velocity field decomposes in a similar way:

$$\mathbf{u}_D(\mathbf{x};N) = \mathbf{U}_\infty(\mathbf{x}) + \tilde{\mathbf{u}}_D(\mathbf{x};N), \tag{33}$$

with, as before, $\tilde{\mathbf{u}}_D$ periodic.

Since the system is uniform, every field is equal to its volume average and therefore, in particular, the mean volumetric flux (10) may be written

$$\mathbf{u}_m = \mathbf{U}_\infty + \frac{1}{N!}\int \mathrm{d}\mathscr{C}^N \, P_0(N)\left[\frac{1}{V}\int \mathrm{d}^3x\left(\chi_C\tilde{\mathbf{u}}_C + \chi_D\tilde{\mathbf{u}}_D\right)\right]. \tag{34}$$

For each configuration, the quantity in brackets is just the volume average of the periodic part of the exact 'microscopic' volumetric flux for that configuration and can readily be calculated. The remaining integration in configuration space is effected in practice by generating a large number of different configurations and averaging the volume-averaged volumetric flux over them, which is effectively a form of Monte Carlo integration. Configurations are generated by arranging the $N$ spheres randomly in the fundamental cell. The factor $N!$ corresponds to a renumbering of the particles and can simply be ignored.

A relation such as (34) increases the rate of convergence to the mean and reduces the calculation of an average quantity — that, according to the original definition (1), would be quite laborious — to much more readily computable volume averages. This is a central feature which it is essential to retain in the non-uniform case as well so as to make the calculation of ensemble averages practical. To this end, we keep the concept of the infinite repetition of a fundamental cell but use a suitable non-uniform particle probability distribution. The way in which this probability distribution is generated can be explained as follows.

[4] From now on, $N$ will denote the number of particles in the fundamental cell rather than the total number of particles in the system.

Consider a volume $\Delta\mathscr{V}$ of the configuration space of the system. The fraction of systems of a uniform ensemble contained in $\Delta\mathscr{V}$ is given by

$$\int_{\Delta\mathscr{V}} \mathrm{d}\mathscr{C}^N\, P_0(N), \tag{35}$$

where $P_0$ is the uniform probability distribution introduced before. Subject now the center $\mathbf{y}^\alpha$ of each sphere to a small displacement $\mathbf{y}^\alpha \to \mathbf{y}^\alpha - \epsilon\mathbf{F}(\mathbf{y}^\alpha)$, where $\mathbf{F}$ is a given deterministic vector function and $\epsilon$ a small parameter. The fraction of systems in $\Delta\mathscr{V}$ then becomes

$$\int_{\Delta\mathscr{V}} \mathrm{d}\mathscr{C}^N\, P_0(N) + \epsilon \int_{\Delta\mathscr{S}} d\mathscr{C}^N\, P_0(N)\mathbf{N}\cdot\left(\sum_{\alpha=1}^{N}\mathbf{F}\left(\mathbf{y}^\alpha\right)\right)$$

$$= \int_{\Delta\mathscr{V}} \mathrm{d}\mathscr{C}^N\, P_0(N)\left[1 + \epsilon\sum_{\alpha}^{N}\nabla_\alpha\cdot\mathbf{F}\left(\mathbf{y}^\alpha\right)\right], \tag{36}$$

where $\mathbf{N}$ is the unit normal in phase space outwardly directed with respect to the surface $\Delta\mathscr{S}$ of $\Delta\mathscr{V}$, the divergence theorem has been used to obtain the second form, and $\nabla_\alpha$ denotes differentiation with respect to the coordinate $\mathbf{y}^\alpha$ of the $\alpha$th particle. We thus see that the ensemble generated by the displacement of the particles has the probability density[5]

$$P(N) = P_0\left[1 + \epsilon\Phi(N)\right], \tag{37}$$

where

$$\Phi(N) = \sum_{\alpha=1}^{N}\nabla_\alpha\cdot\mathbf{F}\left(\mathbf{y}^\alpha\right). \tag{38}$$

This is of course a well-known result in the theory of probability. Its utility here is twofold. In the first place, it enables us to obtain a specific non-uniform probability density $P(N)$ starting from the readily generated uniform probability $P_0(N)$. Secondly, — and more importantly — the presence of the small parameter $\epsilon$ enables us to readily identify in all the equations the terms due to the spatial nonuniformity of the suspension. The key role played by this feature will become apparent in the following.

In order for $P(N)$ to be periodic it is necessary that $\mathbf{F}$ have the same spatial periodicity as the fundamental cell. We take

$$\nabla\cdot\mathbf{F}(\mathbf{y}) = \sin\mathbf{k}\cdot\mathbf{y} \tag{39}$$

where the direction of $\mathbf{k}$ is along one of the sides of the fundamental cell and its modulus $k$ equals $2\pi$ divided by the length $L$ of the side of the cell in that direction. With this choice average quantities, while not constant, can be represented over the fundamental cell by a Fourier series, the coefficients of which are given by projections, i.e. volume integrals, over

[5] It is evident that, by construction, the non-uniform probability $P$ satisfies the same normalization as $P_0$.

suitable basis functions. In fact, the relation (34) itself can be interpreted as one such projection. In this way the calculation of ensemble averages is reduced to the calculation of volume integrals over the fundamental cell just as in the spatially uniform case.

It would be possible, of course, to choose functions **F** with spatial frequencies greater than the fundamental one taken in Eq. (39). We do not pursue this possibility for reasons of simplicity — to limit the number of Fourier coefficients — and also because we are interested here in small values of $ka$ as will be seen below.

Upon inserting Eq. (39) into the definition (4) of particle number density, we find

$$n(\mathbf{x}) = n^0 + \epsilon n^s \sin \mathbf{k}\cdot\mathbf{x} + \epsilon n^c \cos \mathbf{k}\cdot\mathbf{x} + \cdots, \tag{40}$$

with

$$n^0 = \frac{N}{V}, \tag{41}$$

$$n^s = \frac{2}{V}\frac{1}{N!}\int \mathrm{d}\mathscr{C}^N\, P_0(N)\Phi^2(N), \qquad n^c = \frac{2}{V}\frac{1}{N!}\int \mathrm{d}\mathscr{C}^N\, P_0(N)\Phi(N)\sum_{\alpha=1}^{N}\cos \mathbf{k}\cdot\mathbf{y}^\alpha. \tag{42}$$

The second integral vanishes and, for the first one, a simple calculation gives

$$n^s = \frac{n_0}{L^3} S_N(\mathbf{k}) \tag{43}$$

where $S_N$ is the static structure factor for $N$ hard spheres defined by (see e.g. Allen and Tildesley, 1987; Balucani and Zoppi, 1994)

$$S_N(\mathbf{k}) = 1 + n_0 \int \mathrm{d}^3 r \big[g_N(\mathbf{r}) - 1\big] \exp \mathrm{i}\mathbf{k}\cdot\mathbf{r}, \tag{44}$$

in which $g_N(\mathbf{r})$ is the pair distribution function of the $N$ spheres.

Similarly to Eq. (40), we have

$$\beta_D = \beta_D^0 + \epsilon \beta_D^s \sin \mathbf{k}\cdot\mathbf{x}, \tag{45}$$

where we have dropped the vanishing contribution proportional to $\cos \mathbf{k}\cdot\mathbf{x}$; here

$$\beta_D^0 = N\frac{v}{V}, \tag{46}$$

and, from Eq. (5),

$$\beta_D^s = \left(1 - \frac{a^2k^2}{10}\right) v n^s. \tag{47}$$

For convenience in the manipulations that follow, let

$$\epsilon_s = \epsilon \sin \mathbf{k}\cdot\mathbf{x}, \qquad \epsilon_c = \epsilon \cos \mathbf{k}\cdot\mathbf{x}, \tag{48}$$

and note that

$$\nabla\epsilon_s = k\mathbf{m}\epsilon_c; \qquad \nabla\epsilon_c = -k\mathbf{m}\epsilon_s, \tag{49}$$

where

$$\mathbf{m} = \frac{\mathbf{k}}{k}, \tag{50}$$

is a unit vector in the direction of the nonuniformity of the particle distribution. A truncated Fourier series expansion similar to Eq. (40) will be used for all the field variables; for example

$$\bar{\mathbf{w}} = \mathbf{w}^0 + \epsilon_s\mathbf{w}^s + \epsilon_c\mathbf{w}^c \tag{51}$$

## 6. Mean pressure and volumetric flux in a periodic suspension

Our intent in this paper is to study the average value of the flow quantities in suspensions in which the particles are arranged according to a specific probability distribution. The calculation of particle averages, such as the mean particle velocity $\bar{\mathbf{w}}$ or the mean particle angular velocity $\bar{\boldsymbol{\Omega}}$, from the results of the numerical simulation is of course completely straightforward. The calculation of continuous-phase averages, such as $\langle\mathbf{u}_C\rangle$, $\langle p_C\rangle$, or quantities related to them, such as the volumetric flux $\mathbf{u}_m$ or the mixture pressure $p_m$, on the other hand, is more difficult. Mo and Sangani (1994) give an explicit expression for $\mathbf{u}_m$ for the uniform case (their Eq. (69)), that they obtain by an application of the divergence theorem. Unfortunately, the same method does not work in the present non-uniform case and a direct calculation is more involved. We present such a calculation in another paper (Tanksley et al., 1999), both in view of its intrinsic interest and as a check on the present results, but here we follow a more direct route that is based on the averaged momentum equation (31). The basis of this calculation is the Fourier-series structure of all the average quantities expected when the ensemble is constructed as described in the previous section.

We study three distinct physical situations, but it will be sufficient to present details for the first one only.

### 6.1. Sedimentation

In the first flow that we simulate, the motion of the particles is induced by a body force $\mathbf{g}$. Under the action of this force, in a quiescent fluid, an isolated particle would move with a velocity $\mathbf{W}$ given by

$$\mathbf{W} = \frac{2}{9}a^2\frac{\rho_D - \rho_C}{\mu_C}\mathbf{g} \tag{52}$$

We use this relation to eliminate the vector $\mathbf{g}$ in the following equations.

Upon taking the divergence of the momentum equation (31), recalling that $\nabla\cdot\mathbf{u}_m = 0$ because both phases are incompressible, and the sinusoidal dependence (40) of the particle

number density $n$, we find

$$\nabla^2 p_m = \nabla\nabla{:}\boldsymbol{\Sigma}_P + \frac{9}{2a^2}\mu_C k\beta^s \epsilon_c \mathbf{W}\cdot\mathbf{m}. \tag{53}$$

where $\beta^s = vn^s$. Write

$$\frac{1}{\mu_C}\boldsymbol{\Sigma}_P = \mathbf{L}^0 + \epsilon_s \mathbf{L}^s + \epsilon_c \mathbf{L}^c, \tag{54}$$

and note that $\nabla\nabla{:}\mathbf{L}^0 = 0$ since $\nabla\cdot\mathbf{L}^0$ is the divergence of the stress for a uniform suspension and is therefore a constant. The quantities $\mathbf{L}^{s,c}$ will be suitably parameterized and, as several others introduced later, calculated numerically. The solution of Eq. (53) is then[6]

$$\frac{1}{\mu_C}p_m = \beta_D^0 \frac{9}{2a^2}\mathbf{W}\cdot\mathbf{x} - \frac{9}{2ka^2}\beta^s\epsilon_c \mathbf{W}\cdot\mathbf{m} + \mathbf{m}\cdot(\mathbf{L}^s\epsilon_s + \mathbf{L}^c\epsilon_c)\cdot\mathbf{m}, \tag{55}$$

where the first term (to which this expression reduces for $\epsilon = 0$), is found from a consideration of the momentum equation (31) in the special case of a uniform suspension (see Mo and Sangani, 1994).[7]

Upon substituting this expression into Eq. (31) and solving, one finds the following result for the mean volumetric flux:

$$\mathbf{u}_m - \mathbf{U}_\infty = (\mathbf{I}-\mathbf{mm})\cdot\left[\frac{9}{2k^2a^2}\beta^s\epsilon_s\mathbf{W} + \frac{1}{k}(\mathbf{L}^s\epsilon_c - \mathbf{L}^c\epsilon_s)\cdot\mathbf{m}\right], \tag{56}$$

where $\mathbf{U}_\infty$ is the volumetric flow rate of the suspension averaged over planes perpendicular to $\mathbf{m}$. One could eliminate this vector by explicitly adopting a specific frame of reference. However, in order to exhibit the frame invariance of our results, we prefer not to do so.

The expressions for $p_m$ and $\mathbf{u}_m$ may be made more definite by observing that there are two fundamental vectors, $\mathbf{W}$ and $\mathbf{m}$, that can be combined to give the equivalent pair

$$\mathbf{W}^{\parallel} = (\mathbf{W}\cdot\mathbf{m})\mathbf{m}, \qquad \mathbf{W}^{\perp} = (\mathbf{I}-\mathbf{mm})\cdot\mathbf{W}. \tag{57}$$

Since there would be no motion for $\mathbf{W} = 0$ (i.e., $\mathbf{g} = 0$), and since the problem is linear, the velocity fields must depend linearly on these vectors. By a similar argument, the fundamental two-tensors available to express $\boldsymbol{\Sigma}_P$ are

$$\mathbf{G}_S^W = \mathbf{W}^{\perp}\mathbf{m} + \mathbf{m}\mathbf{W}^{\perp}, \qquad \mathbf{G}_A^W = \mathbf{W}^{\perp}\mathbf{m} - \mathbf{m}\mathbf{W}^{\perp},$$

$$\mathbf{G}_I^W = (\mathbf{W}\cdot\mathbf{m})\mathbf{I}, \qquad \mathbf{G}_M^W = (\mathbf{W}\cdot\mathbf{m})\left(\mathbf{mm} - \frac{1}{3}\mathbf{I}\right). \tag{58}$$

[6] In principle, we should write $p_m - P_\infty$ where $P_\infty$ is the pressure field corresponding to $\mathbf{U}_\infty$. For the $\mathbf{U}_\infty$ considered here, however, $P_\infty$ is a constant and, since $p_m$ is defined up to a constant by construction (see Marchioro et al., 1999), this is unnecessary.

[7] The tensor $\mathbf{L}^0$ in this case is evidently isotropic and is represented by the first term in (55).

We can therefore write, with the superscript $j = s$ or $c$,

$$k\mathbf{L}^{j} = \ell_S^{j}\mathbf{G}_S^{W} + \ell_A^{j}\mathbf{G}_A^{W} + \ell_I^{j}\mathbf{G}_I^{W} + \ell_M^{j}\mathbf{G}_M^{W}, \tag{59}$$

where the factor $k$ has been introduced so as to make the coefficients $\ell_j$ dimensionless. These coefficients will be found numerically in the manner described in Section 7. It should be expressly noted that the validity of relations such as Eq. (59) is critically dependent on the absence of privileged directions in space other than those identified by $\mathbf{m}$ and $\mathbf{W}$. In particular, if the particle probability distribution function were characterized by one or more intrinsic vectors or tensors, the structure of Eq. (59) would be different.

With Eq. (59), we readily find

$$\mathbf{u}_m - \mathbf{U}_\infty = \frac{1}{k^2a^2}\left[\frac{9}{2}\beta^s\epsilon_c - L^c\epsilon_s\right]\mathbf{W}^{\perp}, \tag{60}$$

$$\frac{1}{\mu_C}p_m = \beta_D^0\frac{9}{2a^2}\mathbf{W}\cdot\mathbf{x} + \frac{1}{ka^2}\left[P^c\epsilon_c + \left(\ell_I^s + \frac{2}{3}\ell_M^s\right)\epsilon_s\right](\mathbf{W}^{\parallel}\cdot\mathbf{m}), \tag{61}$$

where, we have set

$$L^{j} = \ell_S^{j} + \ell_A^{j}, \qquad P^c = \ell_I^c + \frac{2}{3}\ell_M^c - \frac{9}{2}\beta^s, \tag{62}$$

for brevity.

Two important quantities involving gradients of $\mathbf{u}_m$ are the mixture vorticity

$$\nabla\times(\mathbf{u}_m - \mathbf{U}_\infty) = -\frac{1}{ka^2}\left[-\frac{9}{2}\beta^s\epsilon_c + L^s\epsilon_s + L^c\epsilon_c\right]\mathbf{m}\times\mathbf{W}^{\perp}, \tag{63}$$

and the rate of strain of the volumetric flux (16):

$$\mathbf{E}_m = \frac{1}{2}\left[\nabla\mathbf{u}_m + (\nabla\mathbf{u}_m)^{\mathrm{T}}\right]. \tag{64}$$

From Eq. (60), we find[8]

$$\mathbf{E}_m = \frac{1}{2ka^2}\left[\frac{9}{2}\beta^s\epsilon_c - L^s\epsilon_s - L^c\epsilon_c\right]\mathbf{G}_S^{W}. \tag{65}$$

Upon substituting the relations (59) into the expression (54) of the particle stress $\boldsymbol{\Sigma}_p$ we have

$$\frac{1}{\mu_C}\boldsymbol{\Sigma}_P + 2\mathbf{E}_m = \frac{1}{ka^2}\left(\frac{9}{2}\beta^s\epsilon_c - \ell_A^c\epsilon_c - \ell_A^s\epsilon_s\right)\mathbf{G}_S^{W} + \frac{1}{ka^2}\sum_{s,c}\left(\ell_A^{j}\mathbf{G}_A^{W} + \ell_I^{j}\mathbf{G}_I^{W} + \ell_M^{j}\mathbf{G}_M^{W}\right)\epsilon_j. \tag{66}$$

[8] Again, as in Eq. (55), in the left-hand side we should write $\mathbf{E}_m - \mathbf{E}_\infty$, where $\mathbf{E}_\infty$ is the rate of strain of the velocity field $\mathbf{U}_\infty$. For simplicity, we omit this term that vanishes when, as here, $\mathbf{U}_\infty$ is a rigid-body motion.

We shall need expressions similar to Eqs. (60) and (61) for other variables as well. Thus, we set

$$\bar{\mathbf{w}} - \mathbf{U}_\infty = \Phi\left(\beta_D^0\right)\mathbf{W} + \frac{1}{k^2a^2}\sum_{j=s,c}\left(w_\perp^j\mathbf{W}^\perp + w_\parallel^j\mathbf{W}^\parallel\right)\epsilon_j, \tag{67}$$

where $\Phi$ is the concentration-dependent hindered settling function for a homogeneous suspension, i.e. the ratio between the particle settling velocity at the volume fraction $\beta_D$ and the settling velocity $\mathbf{W}$ of an isolated particle (see e.g. Hetsroni, 1982; Davis and Acrivos, 1985; Russell et al., 1989). As a consequence of this definition, $\Phi(0) = 1$. Similarly we set

$$\bar{\boldsymbol{\Omega}} - \boldsymbol{\Omega}_\infty = \frac{1}{ka^2}\sum_{j=s,c}\omega^j\epsilon_j\mathbf{m}\times\mathbf{W}^\perp, \tag{68}$$

where $\boldsymbol{\Omega}_\infty = \frac{1}{2}\nabla\times\mathbf{U}_\infty$. The coefficients $w$ and $\omega$ are all dimensionless. Finally, for the average continuous-phase pressure, we write

$$\frac{1}{\mu_C}\langle p_C\rangle = Q^0 + \beta_D^0\frac{9}{2a^2}\mathbf{W}\cdot\mathbf{x} + \frac{1}{ka^2}\left(q^c\epsilon_c + q^s\epsilon_s\right)(\mathbf{W}^\parallel\cdot\mathbf{m}), \tag{69}$$

where $Q^0$ is the absolute level with respect to that of $p_m$.

All the dimensionless coefficients $\ell$, $w$, $\omega$, $q$ introduced here and in the remainder of this section can be computed numerically from the results of the direct numerical simulations. The analysis of the terms proportional to $\epsilon_s$ and $\epsilon_c$, which, by construction, would vanish in the case of a uniform suspension, will reveal the fundamental qualitative differences introduced by the spatial nonuniformity of the system. The manner in which these calculations are carried out is summarized in Section 7.

### 6.2. Simple shear

The second flow we study is induced by an imposed shear, for which

$$\mathbf{U}_\infty = \boldsymbol{\gamma}\cdot\mathbf{x}, \tag{70}$$

where $\boldsymbol{\gamma}$ is a symmetric traceless constant two-tensor specifying the rate of shear. Note that $a\boldsymbol{\gamma}$ has the same dimensions as $\mathbf{W}$. Since inertia is neglected, an arbitrary rigid motion can be added to the right-hand side of Eq. (70) and will be understood in the following. From the tensor $\boldsymbol{\gamma}$ and the vector $\mathbf{m}$, one can form two linearly independent vectors analogous to Eq. (57):

$$\boldsymbol{\gamma}^\parallel = (\mathbf{m}\cdot\boldsymbol{\gamma}\cdot\mathbf{m})\mathbf{m}, \qquad \boldsymbol{\gamma}^\perp = \boldsymbol{\gamma}\cdot\mathbf{m} - (\mathbf{m}\cdot\boldsymbol{\gamma}\cdot\mathbf{m})\mathbf{m}. \tag{71}$$

The possible two-tensors are

$$\begin{aligned}&\boldsymbol{\gamma}, \quad \mathbf{G}_S^\gamma = \boldsymbol{\gamma}^\perp\mathbf{m} + \mathbf{m}\boldsymbol{\gamma}^\perp, \quad \mathbf{G}_A^\gamma = \boldsymbol{\gamma}^\perp\mathbf{m} - \mathbf{m}\boldsymbol{\gamma}^\perp, \quad \mathbf{G}_I^\gamma = \left(\boldsymbol{\gamma}^\parallel\cdot\mathbf{m}\right)\mathbf{I},\\ &\mathbf{G}_M^\gamma = \left(\boldsymbol{\gamma}^\parallel\cdot\mathbf{m}\right)\left(\mathbf{mm} - \frac{1}{3}\mathbf{I}\right).\end{aligned} \tag{72}$$

The last four are analogous to Eq. (58) of the previous case, while the first one is specific for the present situation of imposed shear. Because of this difference, in this case we find

$$\mathbf{L}^0 = \ell^0 a\boldsymbol{\gamma}, \tag{73}$$

while the other relations are similar to Eqs. (59)–(69):

$$k\mathbf{L}^j = \ell_\gamma^j a\boldsymbol{\gamma} + \ell_S^j a\mathbf{G}_S^\gamma + \ell_A^j a\mathbf{G}_A^\gamma + \ell_I^j a\mathbf{G}_I^\gamma + \ell_M^j a\mathbf{G}_M^\gamma, \tag{74}$$

$$\mathbf{u}_m - \mathbf{U}_\infty = \frac{1}{k^2 a}(L^s\epsilon_c - L^c\epsilon_s)\boldsymbol{\gamma}^\perp, \tag{75}$$

$$\frac{1}{\mu_C}p_m = \frac{1}{ka}\left[\left(\ell_I^c + \frac{2}{3}\ell_M^c + \ell_\gamma^c\right)\epsilon_c + P^s\epsilon_s\right](\boldsymbol{\gamma}^\parallel \cdot \mathbf{m}), \tag{76}$$

$$L^j = \ell_S^j + \ell_A^j + \ell_\gamma^j, \qquad P^s = \ell_I^s + \frac{2}{3}\ell_M^s + \ell_\gamma^s, \tag{77}$$

$$\mathbf{E}_m = \boldsymbol{\gamma} - \frac{1}{2ka}(L^s\epsilon_s + L^c\epsilon_c)\mathbf{G}_S^\gamma, \tag{78}$$

$$\frac{1}{\mu_C}\boldsymbol{\Sigma}_P + 2\mathbf{E}_m = (2+\ell^0)\boldsymbol{\gamma} - (\ell_A^s\epsilon_s + \ell_A^c\epsilon_c)\mathbf{G}_S^\gamma + \frac{1}{ka}\sum_{s,c}\left(\ell_A^j\mathbf{G}_A^\gamma + \ell_I^j\mathbf{G}_I^\gamma + \ell_M^j\mathbf{G}_M^\gamma\right)\epsilon_j. \tag{79}$$

$$\bar{\mathbf{w}} - \mathbf{U}_\infty = \frac{1}{k^2 a}\sum_{j=s,c}\left(w_\perp^j\boldsymbol{\gamma}^\perp + w_\parallel^j\boldsymbol{\gamma}^\parallel\right)\epsilon_j, \tag{80}$$

$$\bar{\boldsymbol{\Omega}} = \frac{1}{ka}\sum_{j=s,c}\omega^j\epsilon_j\mathbf{m}\times\boldsymbol{\gamma}^\perp \tag{81}$$

$$\frac{1}{\mu_C}\langle p_C\rangle = Q^0 + \frac{1}{ka}\sum_{j=s,c}Q^j\epsilon_j(\boldsymbol{\gamma}^\parallel\cdot\mathbf{m}). \tag{82}$$

### 6.3. Applied couple

For the third flow that we simulate, each particle is subject to a couple $\mathbf{T}$, under the action of which an isolated particle would rotate with the angular velocity

$$\boldsymbol{\omega} = \frac{1}{6v\mu_C}\mathbf{T}, \tag{83}$$

with respect to the fluid. Note that $a\boldsymbol{\omega}$ and $\mathbf{W}$ have the same dimensions.

One can form two axial vectors:

$$\boldsymbol{\omega}^{\parallel} = (\boldsymbol{\omega}\cdot\mathbf{m})\mathbf{m}, \qquad \boldsymbol{\omega}^{\perp} = (\mathbf{I}-\mathbf{mm})\cdot\boldsymbol{\omega}. \tag{84}$$

The fundamental two-tensors are

$$\mathbf{G}_S^{\omega} = (\mathbf{m}\times\boldsymbol{\omega})\mathbf{m} + \mathbf{m}(\mathbf{m}\times\boldsymbol{\omega}), \qquad \mathbf{G}_A^{\omega} = (\mathbf{m}\times\boldsymbol{\omega})\mathbf{m} - \mathbf{m}(\mathbf{m}\times\boldsymbol{\omega}). \tag{85}$$

Proceeding again as before,

$$k\mathbf{L}^{\,j} = \ell_S^{\,j} a\mathbf{G}_S^{\omega} + \ell_A^{\,j} a\mathbf{G}_A^{\omega}. \tag{86}$$

$$\mathbf{u}_m - \mathbf{U}_\infty = \frac{1}{k^2 a}(L^s\epsilon_c - L^c\epsilon_s)\mathbf{m}\times\boldsymbol{\omega}, \tag{87}$$

$$L^{\,j} = \ell_S^{\,j} + \ell_A^{\,j}, \tag{88}$$

$$\mathbf{E}_m = -\frac{1}{2ka}(L^s\epsilon_s + L^c\epsilon_c)\mathbf{G}_S^{\omega}, \tag{89}$$

$$\frac{1}{\mu_C}\boldsymbol{\Sigma}_P + 2\mathbf{E}_m = \frac{1}{ka}\left[-\left(\ell_A^s\epsilon_s + \ell_A^c\epsilon_c\right)\mathbf{G}_S^{\omega} + \sum_{s,c}\ell_A^{\,j}\epsilon_j\mathbf{G}_A^{\omega}\right]. \tag{90}$$

$$\bar{\mathbf{w}} - \mathbf{U}_\infty = \frac{1}{k^2 a}\sum_{j=s,c} w_{\perp}^{\,j}\epsilon_j\mathbf{m}\times\boldsymbol{\omega} \tag{91}$$

$$\bar{\boldsymbol{\Omega}} - \boldsymbol{\Omega}_\infty = \Psi\left(\beta_D^0\right)\boldsymbol{\omega} + \frac{1}{ka}\sum_{j=s,c}\left[\omega_{\parallel}^{\,j}\boldsymbol{\omega}^{\parallel} + \omega_{\perp}^{\,j}\boldsymbol{\omega}^{\perp}\right]\epsilon_j \tag{92}$$

where $\Psi$ is the hindrance function for rotation (see Brenner, 1970, 1972, 1984).

In the previous two cases we had parameterized $p_m$ in terms of a scalar constructed from the polar vector characterizing the flow ($\mathbf{W}$ or $\boldsymbol{\gamma}^{\parallel}$) dotted into $\mathbf{m}$. In this case, since the only polar vector is $\mathbf{m}\times\boldsymbol{\omega}$, a parallel procedure would give zero and therefore we expect that $p_m = 0$, which is confirmed by the numerical results.

### 6.4. Non-Newtonian nature of a non-homogeneous suspension

By comparing the expressions for $\mathbf{E}_m$ given in Eqs. (65), (78) and (89) with the corresponding expressions for the viscous stress (66), (79) and (90), we recognize that a proportionality relation between the two quantities as required by a Newtonian rheological

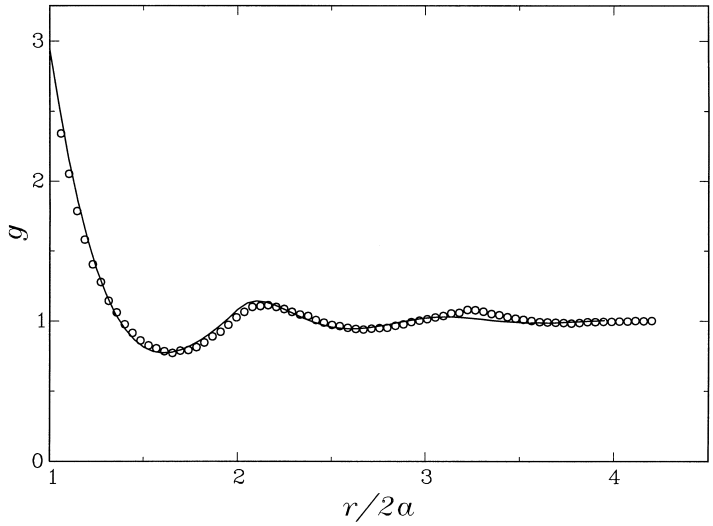


Fig. 1. Comparison of the pair distribution function based on a typical ensemble used in this work (circles) with the solution of the Percus–Yevick equation. The ensemble consists of 2,000 configurations for $\beta_D = 35\%$ and 51 particles.

behavior would only be possible if all the coefficients of the summations in (66), (79) and (90) vanished. The numerical evidence to be discussed in Sections 8–10 shows unambiguously that this would happen only in the case of a uniform suspension. This argument, therefore, proves that the stress in the mixture can be represented in a Newtonian fashion with an effective viscosity only in the random uniform case. For non-uniform suspensions the constitutive relation will necessarily be more complex. This matter is addressed more fully in Part II.

For the reason noted after Eq. (59), this conclusion is only valid because we have explicitly ruled out the presence of privileged directions in space associated to the microstructure of the suspension. It is well known that, if such directions existed, also a uniform suspension would exhibit non-Newtonian behavior.

## 7. Numerical method

The present study exhibits several computational aspects that will now be briefly described in turn.

### *7.1. Configurations*

The ensemble of configurations used in the direct numerical simulation was generated according to a standard Metropolis algorithm (see e.g. Allen and Tildesley, 1987). One starts with the particles arranged in a regular array inside the fundamental cell. Random displacements are then generated for each particle, with the particle actually moved only if the displacement does not cause it to overlap with a neighboring particle. This procedure was

implemented in two ways. In the first one, the scale of the random displacements was dynamically adjusted so that approximately 50% of all attempted moves was accepted. After allowing for an initial transient of the order of $10^6$ displacements per particle, the ensemble was constructed by storing the configurations of the $N$ particles every 20,000 to 100,000 steps per particle. A greater number of steps was taken at the larger volume fractions and particle numbers. The second procedure consisted in adjusting the scale of the displacement so that the acceptance rate was about 90%, which corresponds to approximately one half of the mean interparticle distance. Configurations were stored after 30,000 to 90,000 displacements per particle. These numbers were sufficient to give rise to an approximately Gaussian distribution of particle displacements with a mean equal to one-half the size of the cell. To avoid biases, particles were displaced in random order rather than in a fixed sequence.

As a randomness test of the ensembles of configurations, we have compared the pair distribution function $g(r)$ (where $r$ is the distance from the center of the test particle) for our ensembles with solutions of the Percus–Yevick equation (Throop and Bearman, 1965). Typical results obtained with 2,000 configurations for $\beta_D = 35\%$ and 51 particles are shown in Fig. 1. The Percus–Yevick solution (line) extends to the largest abscissa considered by Throop and Bearman, while the present results (open circles) reach nearly as far as the cell size which, with the present parameters, is $L/2a \simeq 4.24$. The close agreement between theory and computations supports the good quality of the ensembles used in this work.

As a further test, we calculated the nearest-neighbor distribution function $E_p$ for our configurations (open circles in Fig. 2) and compared it with the approximate theoretical result of Torquato and Lee (1990). The result of this comparison for the same case of Fig. 1 is shown in Fig. 2 and again supports the randomness of our ensembles.

Finally, for each ensemble, we can calculate the static structure factor $S_N$ from Eq. (44). It is

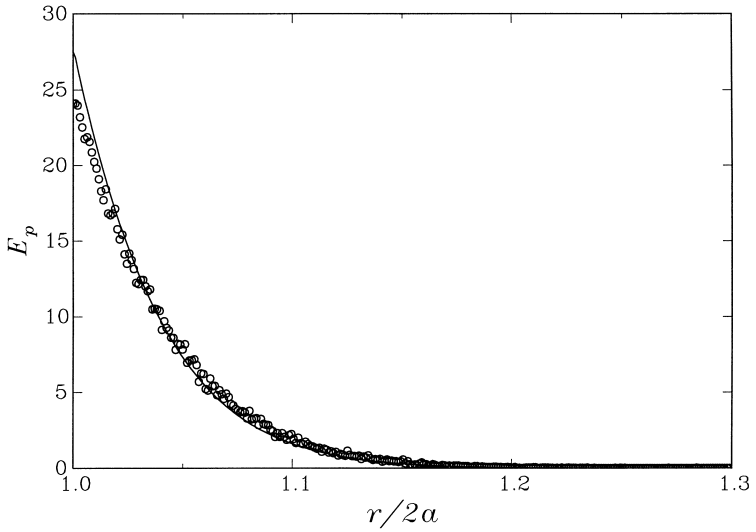


Fig. 2. Nearest-neighbor distribution function for the same ensemble as in the previous figure (open circles) compared with the approximate theoretical result of Torquato and Lee (1990).

known that the difference between $S_N$ and the corresponding quantity $S$ for an infinite number of particles is of order $1/N$ (see e.g. Salacuse et al., 1996), which is a relatively small number in the present calculations. Hence, we can compare our $S_N$ with a suitable approximate expression for $S$. We choose the form given by Studart et al. (1996):

$$S(k) = \frac{2ak}{2ak + 24\beta_D^0 f\left(\beta_D^0\right) j_1(2ak)} \tag{93}$$

where $j_1$ is a spherical Bessel function and

$$f\left(\beta_D^0\right) = \frac{1}{8\beta_D^0}\left(\frac{1}{S(0)} - 1\right). \tag{94}$$

For $S(O)$, we take the higher order Carnahan–Starling approximation (see e.g. Hansen and McDonald, 1990; Mo and Sangani, 1994)

$$S(0) = \frac{\left(1 - \beta_D^0\right)^4}{1 + 4\beta_D^0 + 4\left(\beta_D^0\right)^2 - 4\left(\beta_D^0\right)^3 + \left(\beta_D^0\right)^4}. \tag{95}$$

A comparison between our $S_N$ (symbols) and $S(k)$ (lines) given by Eqs. (93) and (95) is shown in Fig. 3 for $\beta_D^0 = 15\%$ (triangles), 25% (circles), and 35% (squares) with $N$ between 16 and 64.

For a given set of particle arrangements, the effective number of configurations in the ensemble can be increased by suitably orienting the forcing (force, shear, or couple). The force

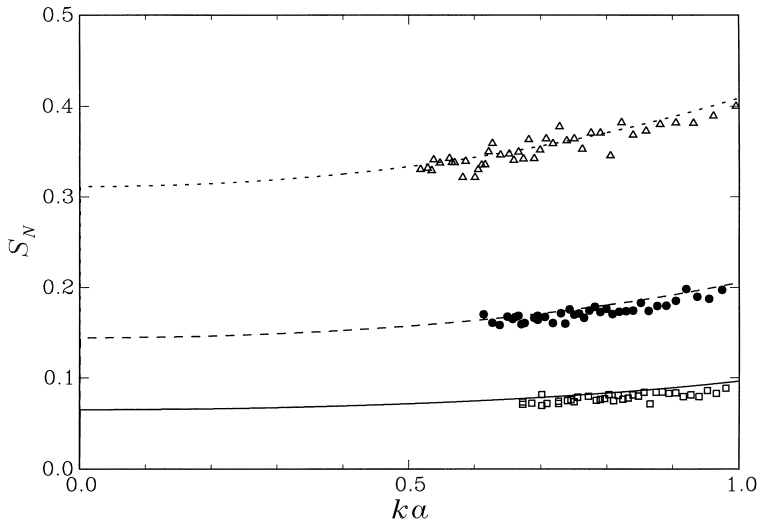


Fig. 3. Static structure factor $S$ as a function of $ka$ for $\beta_D = 15\%$ (triangles), 25% (bullets), and 35% (squares), compared with the approximate expression given by Studart et al. (1996), Eq. (93).

and couple cases are characterized by a vector quantity, **g** or **T**, that we take, in turn, parallel to the three sides of the fundamental cell for a given particle arrangement. For the case of simple shear, we have five independent traceless symmetric tensors of the form

$$\gamma \propto \begin{pmatrix} 1 & 0 & 0 \\ 0 & -1 & 0 \\ 0 & 0 & 0 \end{pmatrix}, \qquad \begin{pmatrix} 0 & 1 & 0 \\ 1 & 0 & 0 \\ 0 & 0 & 0 \end{pmatrix} \text{ etc.} \tag{96}$$

Thus, in the case of applied force and couple, this procedure effectively multiplies by 3 the number of configurations, while in the shear case it multiplies it by 5. An additional factor is gained in some other cases. For instance, by orienting the vector **m** in the two possible directions orthogonal to **g**, we effectively double the number of configurations that contribute to the coefficients of terms proportional to $\mathbf{W}^{\perp}$, and similarly for the shear and couple cases.

### 7.2. Stokes flow solution

Given the particle distribution for each configuration and the imposed velocity field $\mathbf{U}_{\infty}$, the Stokes equations are solved by the singularity method of Mo and Sangani (1994). Our computer code was essentially a rewrite of the original code that was kindly made available to us by Prof. Sangani. The capability to calculate several other quantities, such as the integrals over the particle surfaces appearing in the definition (27) of $p_m$, was also added to the original code.

The solution is expressed in two complementary ways. A global form, useful to handle the particle–particle interactions, consists of the superposition of singularities centered at the particle centers. This global solution is coupled to local solutions, valid in the neighborhood of each particle, taken to have the Lamb (1932) form.

In the implementation of the method the user specifies the number of singularities used in the global solution and the number of terms retained in the Lamb series solution. The magnitude of the computational effort increases rapidly with the number of terms retained. We have mostly used five singularities and, in a few cases, six. Comparing the results we have found that five singularities are sufficient for an accurate solution up to a volume fraction of 25–30%. At 35%, five singularities lead to a loss of accuracy for some coefficients and, therefore, there is the possibility that some of our results at $\beta_D = 35\%$ are not fully converged. Unfortunately, the computational resources available did not permit us to further refine these results.

### 7.3. Calculation of particle averages

The procedure used to calculate the particle averages, defined in (3), can be illustrated with reference to the average center-of-mass velocity $\bar{\mathbf{w}}$. We write

$$n(\mathbf{x})\bar{\mathbf{w}}(\mathbf{x}) = \tilde{\mathbf{w}}^0 + \tilde{\mathbf{w}}^s \sin \mathbf{k}\cdot\mathbf{x} + \tilde{\mathbf{w}}^c \cos \mathbf{k}\cdot\mathbf{x}, \tag{97}$$

where, from Eq. (3), the first Fourier coefficient in the right-hand side is given by

$$\tilde{\mathbf{w}}^0 = \frac{1}{V}\int \mathrm{d}^3x\, n(\mathbf{x})\bar{\mathbf{w}}(\mathbf{x})$$

$$= n^0 \int \mathrm{d}\mathscr{C}^N\, P_0(N)\big[1+\varepsilon\phi(N)\big]\frac{1}{N}\sum_{\alpha=1}^{N}\mathbf{w}^\alpha(N)$$

$$= \mathbf{w}_0^0 + \varepsilon\mathbf{w}_\varepsilon^0, \tag{98}$$

where the last step follows simply by separating the $O(1)$ and $O(\epsilon)$ terms of the integral and we have used Eq. (41) to write $1/V$ as $n_0/N$. Similarly

$$\tilde{\mathbf{w}}^s = n^0 \int \mathrm{d}\mathscr{C}^N\, P_0(N)\big[1+\varepsilon\phi(N)\big]\frac{1}{N}\sum_{\alpha=1}\mathbf{w}^\alpha(N)\sin\mathbf{k}\cdot\mathbf{y}^\alpha = \mathbf{w}_0^s + \varepsilon\mathbf{w}_\varepsilon^s, \tag{99}$$

with a corresponding expression for $\tilde{\mathbf{w}}^c$. Upon substituting into Eq. (97), we thus have

$$n(\mathbf{x})\bar{\mathbf{w}}(\mathbf{x}) = \mathbf{w}_0^0 + \varepsilon\mathbf{w}_\varepsilon^0 + \big(\mathbf{w}_0^s + \varepsilon\mathbf{w}_\varepsilon^s\big)\sin\mathbf{k}\cdot\mathbf{x} + \big(\mathbf{w}_0^c + \varepsilon\mathbf{w}_\varepsilon^c\big)\cos\mathbf{k}\cdot\mathbf{x}. \tag{100}$$

The numerical evidence indicates that $\mathbf{w}_\varepsilon^0$, $\mathbf{w}_0^s$, and $\mathbf{w}_0^c$ are negligible. While we have not been able to prove that they exactly vanish (at least in the limit of an infinitely large ensemble), one would indeed expect that they would. For example, $\mathbf{w}_\varepsilon^0$ could be non-zero only if there were a statistical correlation between the sum of sines in $\phi(N)$ as defined in Eq. (38) and $\sum_\alpha \mathbf{w}^\alpha$. Since the term $\sin\mathbf{k}\cdot\mathbf{y}^\alpha$ of $\phi$ depends on the position of the $\alpha$ particle, while $\mathbf{w}^\alpha$ depends, in addition to the applied deterministic force, on the position of the other particles, and since the particles are uncorrelated (except for the no-overlap constraint) it would be difficult to find a mechanism by which such a statistical correlation could be established. Similarly, since $P_0(N)$ is random, a non-zero value for $\mathbf{w}_0^s$ or $\mathbf{w}_0^c$ would indicate a non-random bias in the distribution of $\sum_\alpha \mathbf{w}^\alpha(N)\sin\mathbf{k}\cdot\mathbf{y}^\alpha$ which, again, would not be expected. If we, therefore, accept that these quantities are exactly zero, and express $n$ in the left-hand side of this relation by means of Eq. (40) (recalling that $n^c = 0$), we may write

$$\bar{\mathbf{w}}(\mathbf{x}) = \frac{1}{n^0 + n^s\varepsilon\sin\mathbf{k}\cdot\mathbf{x}}\big(\mathbf{w}_1^0 + \varepsilon\mathbf{w}_\varepsilon^s\sin\mathbf{k}\cdot\mathbf{x} + \varepsilon\mathbf{w}_\varepsilon^c\cos\mathbf{k}\cdot\mathbf{x}\big)$$

$$= \mathbf{w}^0 + \varepsilon\mathbf{w}^s sin\,\mathbf{k}\cdot\mathbf{x} + \varepsilon\mathbf{w}^c cos\,\mathbf{k}\cdot\mathbf{x} + O(\epsilon^2), \tag{101}$$

where

$$\mathbf{w}^0 = \frac{\mathbf{w}_1^0}{n^0}, \quad \mathbf{w}^s = \frac{\mathbf{w}_s^\varepsilon}{n^0} - \frac{\mathbf{w}_1^0}{n^0}\frac{n^s}{n^0}, \quad \mathbf{w}^c = \frac{\mathbf{w}_c^\varepsilon}{n^0} - \frac{\mathbf{w}_1^0}{n^0}\frac{n^s}{n^0}. \tag{102}$$

Note that all the quantities in these relations are known numerically.

A similar procedure is followed for the other particle averages, and in particular for the tensors $\mathbf{L}^0$, $\mathbf{L}^i$ defined in Eq. (54) and the analogous relations for the shear and couple cases. These quantities are first expressed in terms of averages of the coefficients of the Lamb solution using the definitions (21)–(23) of $\mathscr{T}$ etc. Then these Lamb coefficients averages are expanded in

Fourier series and the relevant Fourier coefficients evaluated as shown before for $\mathbf{w}$. Assembling the various components obtained in this way, $\mathbf{L}^0$, $\mathbf{L}^s$ and $\mathbf{L}^c$ are obtained.

### 7.4. Parameterization of the averages

By the same methods described in Marchioro and Prosperetti (1999), we have verified that the various parameterizations of the average quantities postulated in the previous section is correct. For a simple example illustrating the procedure, consider once more the case of $\bar{\mathbf{w}}$ expanded as in Eq. (101).

For the sedimentation problem $\mathbf{w}$ must be linearly dependent on the driving force, represented by $\mathbf{W}$, and therefore, a priori, it is necessary that

$$\mathbf{w}^0 - \mathbf{U}_\infty = \mathbf{M}^0\left(\beta_D^0, ak\right) \cdot \mathbf{W}, \tag{103}$$

where $\mathbf{M}^0$ is a two-tensor. The numerical results indicate that the off-diagonal elements of $\mathbf{M}^0$ are 3–4 orders of magnitude smaller than the diagonal elements, which in turn differ from each other by a similar amount. Furthermore, the off-diagonal elements fluctuate around 0 as $ka$ is varied.

From these results, we deduce that $\mathbf{M}^0$ is an isotropic tensor, $\mathbf{M}^0 = \Phi\mathbf{I}$, with $\Phi$ the hindered settling function as in (67). This finding implies that the existence of preferential directions parallel to the cell sides, introduced as an artifact of the simulation method, has a negligible effect on the results.

The non-uniform coefficients $\mathbf{w}^s$ and $\mathbf{w}^c$ must also be linearly related to $\mathbf{W}$, but they must only depend on the components of $\mathbf{W}$ parallel and perpendicular to $\mathbf{m}$ and therefore, for example,

$$\mathbf{w}^s = \mathbf{M}_\perp^s\left(\beta_D^0, ak\right) \cdot \mathbf{W}^\perp + \mathbf{M}_\parallel^s\left(\beta_D^0, ak\right) \cdot \mathbf{W}^\parallel, \tag{104}$$

where, again, $\mathbf{M}_\parallel^s$, $\mathbf{M}_\perp^s$ are, a priori, two-tensors. Here, one finds numerically that the off-diagonal elements are about 1% of the diagonal ones, which in turn differ from each other by a similar amount. Due to the fact that the convergence of the ensemble averages for the non-uniform quantities is slower than for the uniform ones — a feature which we have encountered in all our calculations — the numerical evidence for the diagonal nature of the $\mathbf{M}^s$ is less strong than for $\mathbf{M}^0$, but is nevertheless compelling. Thus, we identify the coefficients $w_\parallel^s$, $w_\perp^s$ of Eq. (67) with the traces of $\mathbf{M}_\parallel^s$, $\mathbf{M}_\perp^s$.

The procedure is conceptually similar but gets more cumbersome to implement in the case of the two-tensors $\mathbf{L}^0$, $\mathbf{L}^j$. For example, the linear dependence of $\mathbf{L}^j$ on the tensors $\mathbf{G}_S$, $\mathbf{G}_A$, etc. as written in Eq. (59), a priori, should be expressed in terms of four-tensors. Within our numerical accuracy, these are found to be scalars multiplied by the identity 4-tensor, from which we deduce the coefficients $\ell^j$.

### 7.5. Cell-size dependence

In an ideal implementation of the concept described in Section 5, one would superimpose a

sinusoidal particle distribution upon a truly infinite random suspension. This objective cannot be of course attained in the context of the present method, where the size of the fundamental cell plays a two-fold role: it imposes an artificial periodicity on the background, ideally uniform, particle distribution and, at the same time, gives the scale of variation of the inhomogeneity.

The situation of practical concern in which the macroscopic length scale is much greater than the particle radius corresponds to the limit $ka \to 0$. In this limit the particle distribution as characterized by the probability $P_0$ becomes truly uniform and, at the same time, the scale of variation of the particle inhomogeneity becomes large and the associated gradients correspondingly small. Nevertheless, we are still able to identify the effects of the inhomogeneity as they are singled out by the parameter $\epsilon$.

For each volume fraction several ensembles with different numbers of particles were generated so as to vary the value of the parameter $ka$ expressing the ratio of the particle radius $a$ to the cell size $2\pi/k$. For $N$ particles, and a particle volume fraction of $\beta_D$, $ka$ is given by

$$ka = \left(\frac{6\pi^2}{N}\beta_D\right)^{1/3}, \tag{105}$$

and is therefore a slowly decreasing function of $N$. In general, we used between 16 and 64 particles for each value of $\beta_D$. The values of $ka$ that we could practically attain were, therefore, in the range between 0.5 and 1. Notice that the number of particles necessary to attain a given $ka$ increases with $\beta_D$. For $\beta_D = 15\%$, in some cases as few as 9 particles in the cell gave results consistent with those found with larger numbers of particles at the same volume fraction.

## 8. Results: sedimentation

We describe in this and in the following sections some of the qualitative aspects in which a non-uniform suspension differs from a uniform one as revealed by the ensemble averaging of the direct numerical simulation results according to the non-uniform probability distribution (37). Before considering the non-uniform case, it is useful to begin from an analysis of the $\epsilon$-independent terms of the formulae in Section 6 which embody the results for a uniform suspension. A comparison of these results with those available in the literature will help validate our method and will also make it easier to appreciate the novel phenomenology introduced by spatial non-uniformities.

It follows from (67) and (56) that, in a uniform suspension, the mean sedimentation velocity of the particles with respect to the volumetric flow rate $\mathbf{u}_m$ is

$$\bar{\mathbf{w}} - \mathbf{u}_m = \Phi(\beta_D)\mathbf{W}. \tag{106}$$

In our numerical simulation the hindrance function $\Phi$ depends, in addition to the volume fraction, also on $ka$. Mo and Sangani (1994) give for this dependence an expression that is valid up to the first order in the ratio of the two-particle correlation length to the cell size:

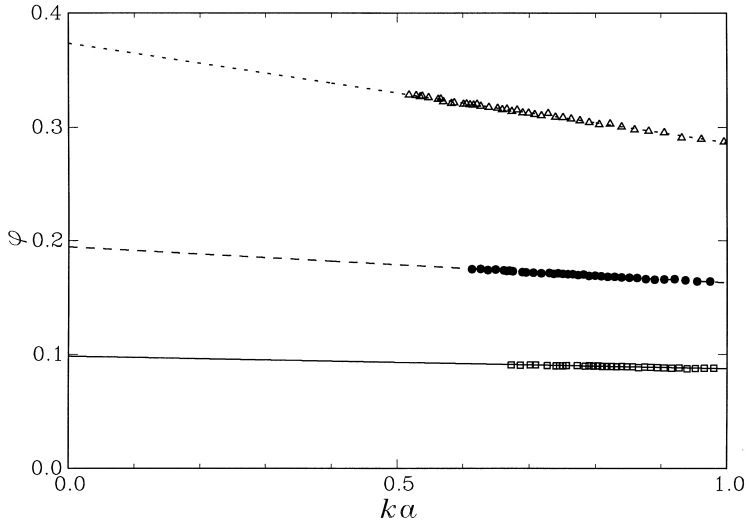


Fig. 4. Numerically computed hindrance settling function as a function of $ka$ for $\beta_D = 15$, 25, and 35%.

$$\Phi\left(\beta_D^0,ka\right) = \Phi\left(\beta_D^0,0\right) - \frac{1.7601}{(6\pi^2)^{1/3}}\frac{\mu_C}{\mu_{\text{eff}}}S(0)ka + O(ka)^3, \tag{107}$$

where $S(0)$ is the structure factor. Typical results for $\Phi(\beta_D^0,ka)$ from our simulations at $\beta_D^0 = 15$, 25, and 35% are shown in Fig. 4 as functions of $ka$. Here, as in all the figures that follow, the triangles are for $\beta_D^0 = 15\%$, the bullets for $\beta_D^0 = 25\%$, and the rectangles for $\beta_D^0 =$

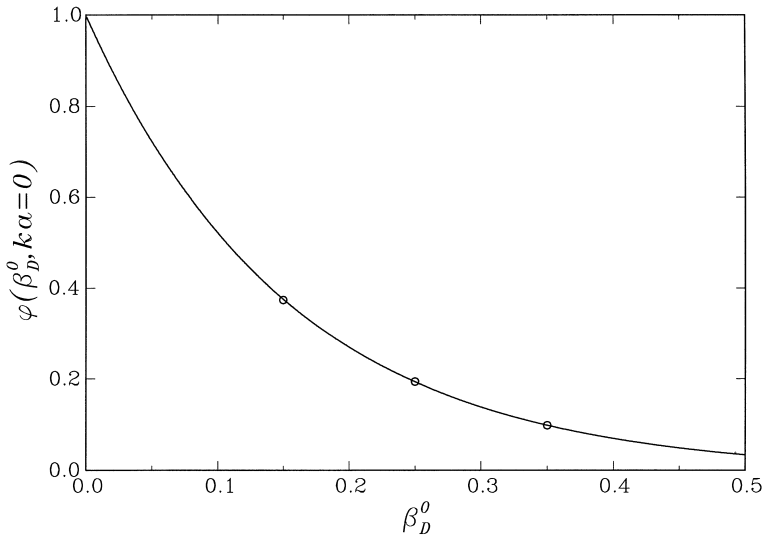


Fig. 5. Values of the numerically computed hindrance settling function of the previous figure extrapolated to $ka = 0$ as a function of $\beta_D$. The line is the fit (108).

35%. From a linear fit, shown by the lines, to these and similar numerical results obtained at other volume fractions, one can extrapolate to $ka = 0$ with reasonable confidence. The result of this procedure is shown in Fig. 5 and can be correlated by an expression of the form

$$\Phi\left(\beta_D^0,0\right) = \left(1-\beta_D^0\right)^{c_1-c_2\beta_D^0}, \tag{108}$$

with $c_1 = 6.50$, $c_2 = 3.18$. For small $\beta_D^0$ this gives $\Phi(\beta_D^0) \simeq 1 - 6.50\beta_D^0$ in good agreement with Batchelor's (1972) well-known result $\Phi(\beta_D,0) = 1 - 6.55\beta_D^0$. Fits of the form $\Phi = (1-\beta_D^0)^n$ do not give an equally good representation of the numerical result.

From the straight-line fit to the data of Fig. 4, according to Eq. (107), one can also deduce a value for $S(0)\mu_C/\mu_{\text{eff}}$ and therefore, knowing $S(0),\mu_{\text{eff}}/\mu_C$. If $S(0)$ is taken to be given by the Carnahan–Starling approximation (95), we find the results shown by the squares in Fig. 6; the other symbols will be discussed below. The solid line in the figure is a fit of the form (Barnes et al., 1989; Phillips et al., 1992)

$$\frac{\mu_{\text{eff}}}{\mu_C} = \left(1-\frac{\beta_D^0}{\beta_{\max}}\right)^{-\theta}, \tag{109}$$

with $\beta_{\max} = 0.79$, $\theta = 1.94$, to results described in the next section. This curve is consistent with the results of Mo and Sangani (1994) and others in the literature. The values of $\mu_{\text{eff}}$ deduced from Eq. (107) agree reasonably well with the line given by Eq. (109) for $\beta_D = 15\%$, but they deviate for increasing $\beta_D$ where the two-particle correlation length ceases to be small in comparison with the cell size.

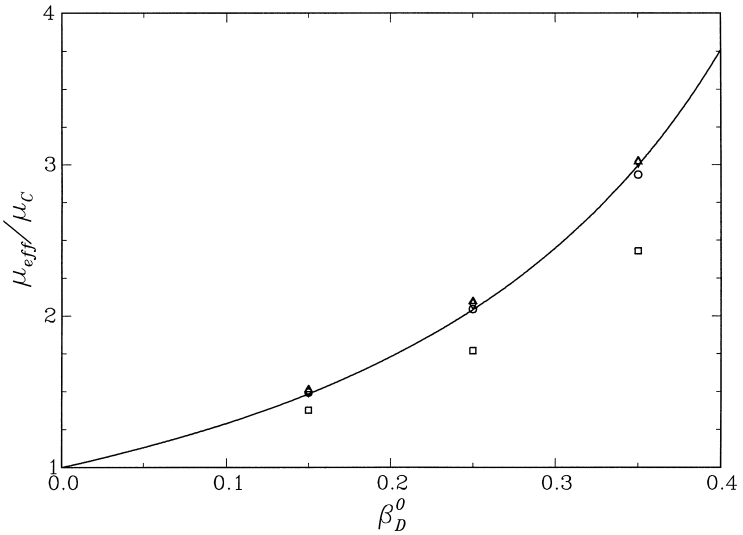


Fig. 6. The normalized effective viscosity of the suspension $\mu_{\text{eff}}/\mu_C$ as a function of particle volume fraction as computed for several flows: □, from Eq. (107); ○, from Eq. (134); △, from Eq. (135); ◇, from Eq. (160). The solid line in the figure is the fit of Eq. (109).

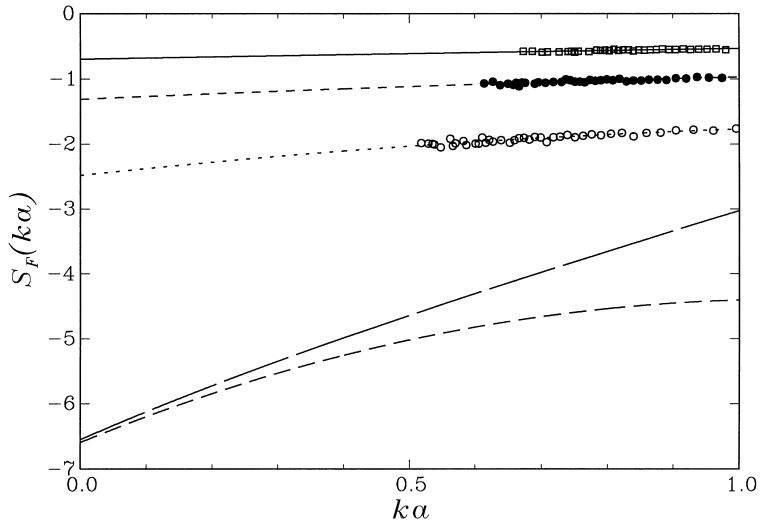


Fig. 7. Feuillebois's result for $vS_F(ka)$, valid as $\beta_D^0 \to 0$ (long dashes) compared with the present numerical results at $\beta_D^0 = 15\%$ (triangles), 25% (bullets), and 35% (squares). The short-dashed line is an extrapolation of our numerical results to $\beta_D^0 = 0$.

For a uniform suspension the difference $p_m - \langle p_C \rangle$ as given by Eq. (69) is

$$p_m - \langle p_C \rangle = -\mu_C Q^0. \tag{110}$$

Our numerical simulations consistently give for $Q^0$ numbers of the order of $10^{-4}$–$10^{-5}$, to be compared e.g. with $p_m/\mu_C$ which is typically a number of order 1. We can therefore conclude that

$$Q^0 = 0, \tag{111}$$

which entails that, for a uniform suspension, $p_m = \langle p_C \rangle = \overline{p^e}$.

Feuillebois (1984) studied the settling of a dilute suspension with a spatial concentration consisting of a vertically varying sinusoidal component superimposed on a uniform distribution $n^0$. His result for the particle settling velocity may be written in the form

$$\frac{w - U_\infty}{|\mathbf{W}|} = 1 - 6.55vn^0 + S_F(ka)v\big[n(\mathbf{x}) - n^0\big], \tag{112}$$

where $S_F$ is a function of $ka$ defined in his paper.[9] Our expression (67) can be put in a similar form, namely

$$\frac{w - U_\infty}{|\mathbf{W}|} = \Phi\big(n^0 v, ka\big) + \frac{w_\parallel^s}{vn^s k^2 a^2} v\big[n(\mathbf{x}) - n^0\big] \tag{113}$$

[9] We use the symbol $S_F$ to denote the same function denoted by $S$ in Feuillebois's paper to avoid confusion with the static structure factor introduced earlier.

In Fig. 7, we show as a function of $ka$ Feuillebois's result for the function $S_F(ka)$ (long dashes) and our numerical results for the analogous quantity multiplying $v[n(\mathbf{x}) - n^0]$ at three volume fractions. These quantities are not directly comparable in this form in view of the strong $\beta_D$ dependence. However, we can use our results to extrapolate to zero volume fraction and then compare with Feuillebois's. To this end, we write

$$\frac{w_{\parallel}^{s}}{vn^{s}k^2a^2} = c_1\left(1-\beta_D^0\right)^{c_2+c_3\beta_D^0}, \tag{114}$$

and evaluate the fitting constants $c_1$, $c_2$, $c_3$ by using the computed results for $\beta_D^0 = 15$, 25, and 35%. Since, in Feuillebois's work, the sinusoidal disturbance is superimposed on a truly random uniform distribution while, in the present one, it is superimposed on the artificially periodic structure of the infinitely repeated fundamental cells, the two situations are not precisely comparable. Nevertheless, there is a general agreement between Feuillebois's result and ours (short dashes).

The numerical simulations indicate that all the coefficients $\ell$ with superscript $s$ vanish. Likewise, we find $w_{\perp}^{c} = w_{\parallel}^{c} = 0$. The previous equation (60) then becomes

$$\mathbf{u}_m - \mathbf{U}_\infty = \frac{1}{k^2a^2}U^{s}\epsilon_s\mathbf{W}^{\perp}, \tag{115}$$

where

$$U^{s} = \frac{9}{2}\beta^{s} - \left(\ell_S^c + \ell_A^c\right), \tag{116}$$

which shows that $\mathbf{u}_m$ differs from the volumetric flow rate of a uniform suspension $\mathbf{U}_\infty$ only

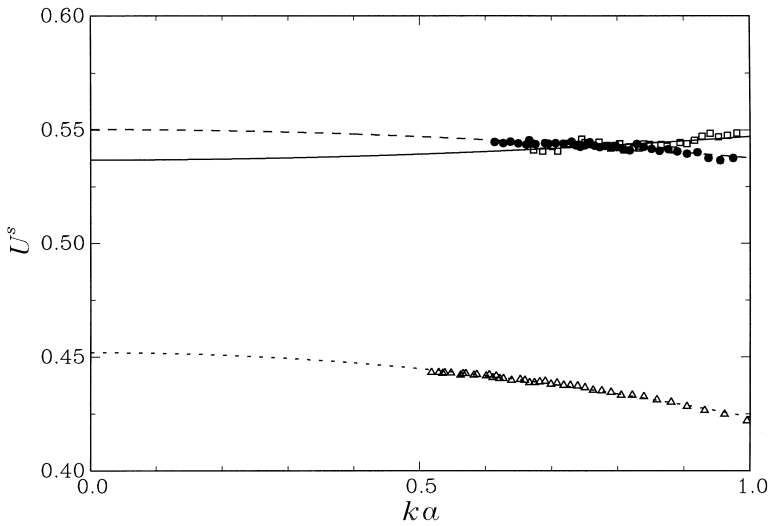


Fig. 8. The coefficient $U^{s}$ appearing in Eq. (115) versus $ka$ for $\beta_D^0 = 15\%$ (triangles), 25% (bullets), and 35% (squares) together with least-squares fits of the form (117).

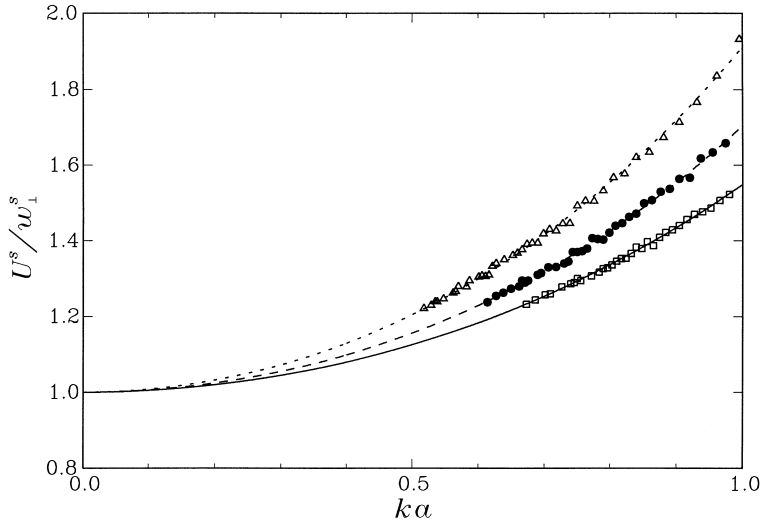


Fig. 9. Ratio $|\mathbf{u}_m|/|\bar{\mathbf{w}}_m|$ as a function of $ka$ for $\beta_D^0 = 15\%$ (triangles), 25% (bullets), and 35% (squares).

when the inhomogeneity is perpendicular to $\mathbf{W}$, i.e. the particles are arranged in vertical sheets of alternatively denser and lighter concentration. This result has an obvious physical interpretation. A graph of the coefficient $U^s$ versus $ka$ is shown in Fig. 8 for $\beta_D^0 = 15$, 25, and 35%, where the lines represent least-squares fits of the form

$$U^s = \gamma + \delta(ak)^2. \tag{117}$$

Since $\gamma \neq 0$, it is clear from Eq. (115) that $\mathbf{u}_m - \mathbf{U}_\infty$ diverges as $ka \to 0$ when $\mathbf{W}^\perp \neq 0$ i.e. when the inhomogeneity is perpendicular to the driving force. This fact is expected as, in this case, the region of heavier mixture becomes wider and wider with decreasing $k$ while the shear force that tends to retard its motion remains constant.[10] The result is supported by the analytical one given in Appendix A for the dilute case.

The representation (67) for the disperse-phase velocity becomes

$$\bar{\mathbf{w}} - \mathbf{U}_\infty = \Phi\left(\beta_D^0, ka\right)\mathbf{W} + \frac{1}{k^2a^2}\left(w_\perp^s \mathbf{W}^\perp + w_\parallel^s \mathbf{W}^\parallel\right)\epsilon_s. \tag{118}$$

Since $w_\perp^s$ and $w_\parallel^s/k^2a^2$ tend to constants in the limit $k \to 0$, we find numerically the same divergence for $\bar{\mathbf{w}}$ as noted before for $\mathbf{u}_m$ provided $\mathbf{W}^\perp \neq 0$. An important physical quantity is the relative or 'slip' velocity

$$\mathbf{u}_\Delta = \bar{\mathbf{w}} - \mathbf{u}_m \tag{119}$$

that must be a Galilean invariant. It is important to verify this property, and all the more so as

[10] One may visualize the situation as a series of vertical heavy "slabs" of more concentrated suspension. The fall of the slabs is retarded by the viscous force on their surfaces. As $ka$ is decreased, the width — and hence the weight — of the slabs increases, but the retarding viscous force does not.

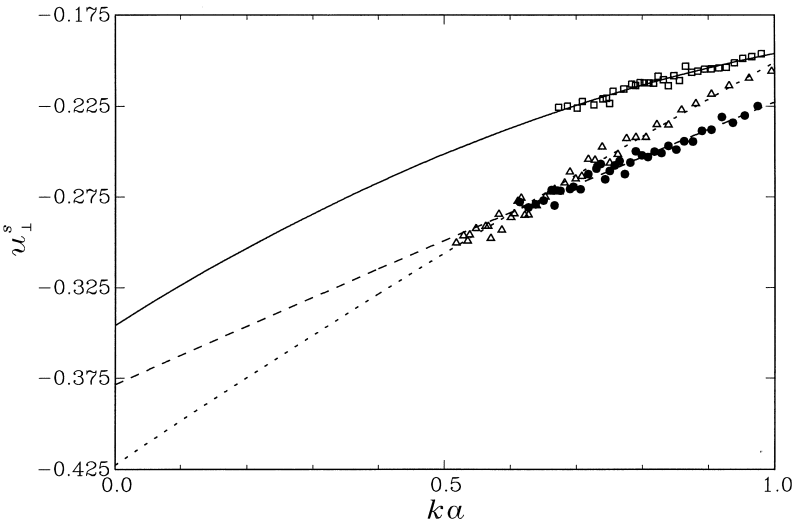


Fig. 10. The coefficient $u_\perp^s$ in Eq. (120) as a function of $ka$ for $\beta_D^0 = 15\%$ (triangles), 25% (bullets), and 35% (squares). The lines are a three-term quadratic fit.

the two velocities in the right-hand side individually diverge in the limit of small $k$. Such a comparison is shown in Fig. 9 in the form of the ratio $U^s/w_\perp^s$. Least-squares fits of the form (117) extrapolated to $ka = 0$ all differ from 1 by only a few percent, which is of the order of the expected numerical accuracy in these simulations. For this reason the lines shown in this figure are of the form $1 + \delta(ka)^2 + \zeta(ka)^4$ with the parameters $\delta,\zeta$ obtained from a least-squares minimization. It is seen that this procedure provides a good representation of the numerical results. On the basis of this result, we write

$$\mathbf{u}_\Delta = \Phi(\beta_D, ka)\mathbf{W} + \left(u_\parallel^s \mathbf{W}^\parallel + u_\perp^s \mathbf{W}^\perp\right)\epsilon_s, \tag{120}$$

where

$$u_\parallel^s = \frac{w_\parallel^s}{k^2a^2}, \qquad u_\perp^s = \frac{1}{k^2a^2}\left(w_\perp^s - U^s\right). \tag{121}$$

The quantities $u_\perp^s$ and $u_\parallel^s$ are shown in Figs. 10 and 11; note that they both approach nonzero constants as $ka \to 0$. In this case the lines are three-term quadratic fits including the linear term $ak$.

The expression (61) for the mean pressure is

$$\frac{1}{\mu_C} p_m = \beta_D^0 \frac{9}{2a^2}\mathbf{W}\cdot\mathbf{x} + \frac{1}{ka^2} P^c \epsilon_c (\mathbf{W}^\parallel \cdot \mathbf{m}). \tag{122}$$

The numerically calculated value of $P^c$ is plotted in Fig. 12 for the three cases $\beta_D^0 = 15$, 25, and 35% as function of $ka$. The lines are a three-term quadratic fit. Since $Q^0 = 0$, the disperse-phase pressure $\langle p_C \rangle$ given by Eq. (69) reduces to

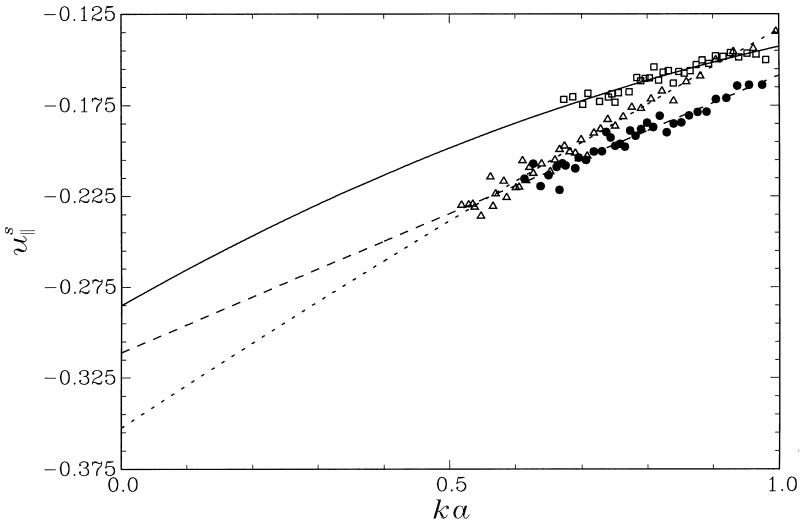


Fig. 11. The coefficient $u_{\parallel}^{s}$ in Eq. (120) as a function of $ka$ for $\beta_D^0 = 15\%$ (triangles), 25% (bullets), and 35% (squares). The lines are a three-term quadratic fit.

$$\frac{1}{\mu_C}\langle p_C\rangle = \beta_D^0 \frac{9}{2a^2}\mathbf{W}\cdot\mathbf{x} + \frac{1}{ka^2}q^c\epsilon_c(\mathbf{W}^{\parallel}\cdot\mathbf{m}). \tag{123}$$

From Eqs. (122) and (123), we have therefore

$$\frac{1}{\mu_C}\langle p_C\rangle - \beta_D^0\frac{9}{2a^2}\mathbf{W}\cdot\mathbf{x} = \zeta_p\left(\frac{1}{\mu_C}p_m - \beta_D^0\frac{9}{2a^2}\mathbf{W}\cdot\mathbf{x}\right), \tag{124}$$

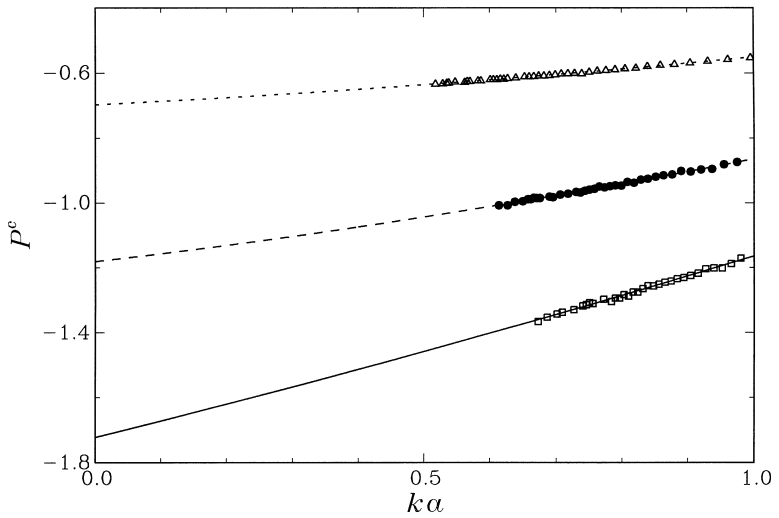


Fig. 12. The coefficient $P^c$ in Eq. (122) as a function of $ka$ for $\beta_D^0 = 15\%$ (triangles), 25% (bullets), and 35% (squares). The lines are a three-term quadratic fit.

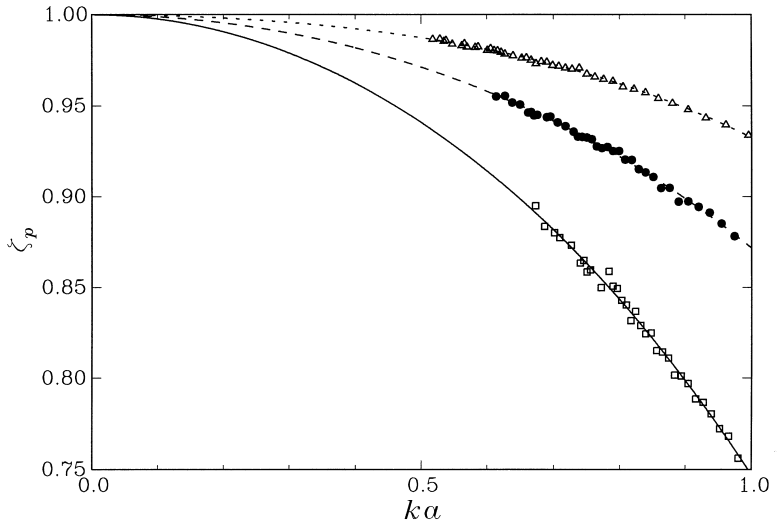


Fig. 13. The coefficient $\zeta_p$ defined in (124) as a function of $ka$ for $\beta_D^0 = 15\%$ (triangles), 25% (bullets), and 35% (squares). The lines are biquadratic least-squares fits subject to the condition that $\zeta_p = 1$ at $ka = 0$.

where

$$\zeta_p = \frac{q^c}{P^c}. \tag{125}$$

This quantity is shown in Fig. 13 as a function of $ka$ for several values of $\beta_D^0$. If the results are fitted as in Eq. (117), for $ka = 0$ one finds a limit value that is essentially 1 and independent of $\beta_D^0$. If the suggested independence of $\beta_D^0$ is correct, the exact result for $ka = 0$ should be the same as the dilute-limit one given in Appendix A, i.e. 1. The lines in Fig. 13 are biquadratic fits forced to reduce to 1 for $ka = 0$. It is evident that, if $\zeta_p$ deviates from 1 for finite $ka$, for a non-uniform suspension the mean pressure acting on the surface of the particles differs from the continuous-phase mean pressure.

In the frame of reference where $\mathbf{U}_\infty = 0$, the mean angular velocity of the particles and the vorticity of the suspending fluid are both zero for a uniform suspension, but not for a non-uniform one. The numerical evidence indicates that $\omega^s = 0$, and Eq. (68) therefore becomes

$$\bar{\boldsymbol{\Omega}} - \boldsymbol{\Omega}_\infty = \frac{1}{ka^2}\omega^c \epsilon_c \mathbf{m} \times \mathbf{W}^\perp. \tag{126}$$

Since, from Eq. (57), $\mathbf{m} \times \mathbf{W}^\perp = \mathbf{m} \times \mathbf{W}$, this equation shows that there is a non-zero mean particle rotation normal to the (**W**,**m**) plane induced by the concentration gradient in the direction orthogonal to the settling velocity, a fact that admits of a ready physical interpretation. The coefficient $\omega^c$ is plotted in Fig. 14.

From Eq. (115), we see that the concentration gradient also induces a mean vorticity and we find the relation

$$\bar{\boldsymbol{\Omega}} - \boldsymbol{\Omega}_\infty = \zeta_\Omega \left( \frac{1}{2} \nabla \times \mathbf{u}_m - \boldsymbol{\Omega}_\infty \right), \tag{127}$$

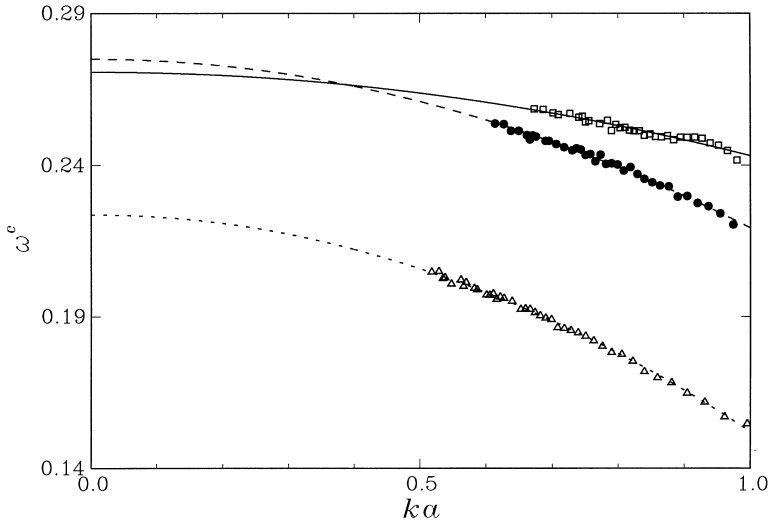


Fig. 14. The coefficient $\omega^c$ of Eq. (126) as a function of $ka$ for $\beta_D^0 = 15\%$ (triangles), 25% (bullets), and 35% (squares). The lines are least-squares fits of the form (117).

where

$$\zeta_\Omega = \frac{2\omega^c}{U^s}. \tag{128}$$

This quantity is shown as a function of $ka$ in Fig. 15. As in the case of $\zeta_p$ considered before, the lines are fitted requiring that $\zeta_\Omega = 1$ for $ka = 0$, as suggested by the dilute-limit analysis of

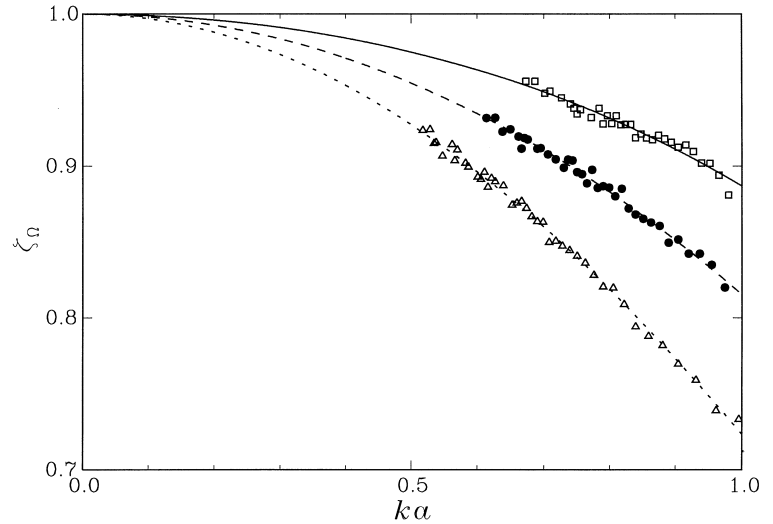


Fig. 15. The coefficient $\zeta_\Omega$ defined in Eq. (127) as a function of $ka$ for $\beta_D^0 = 15\%$ (triangles), 25% (bullets), and 35% (squares). The lines are biquadratic least-squares fits subject to the condition that $\zeta_\Omega = 1$ at $ka = 0$.

Appendix A. Thus, the mean particle angular velocity relative to the mean vorticity vanishes in the limit of a uniform suspension as expected. Furthermore, as for $\mathbf{u}_\Delta$, the divergence in the mean particle angular velocity as $ka \to 0$ is exactly cancelled by a similar divergence of the mean vorticity. We define a slip angular velocity:

$$\boldsymbol{\Omega}_\Delta = \bar{\boldsymbol{\Omega}} - \frac{1}{2}\nabla \times \mathbf{u}_m, \tag{129}$$

that can be expressed as

$$\boldsymbol{\Omega}_\Delta = k\Omega^c \epsilon_c \mathbf{m} \times \mathbf{W}^\perp, \tag{130}$$

where

$$\Omega^c = \frac{1}{k^2 a^2}\left(\omega^c - \frac{1}{2}U^s\right) \tag{131}$$

tends to a nonzero constant as $ka \to 0$ as shown in Fig. 16. The slip translational and rotational velocities defined here, together with similar quantities defined for the other two problems, will play an important role in Part II when we close the system of equations.

The expressions (65) and (66) for the mixture rate of strain and stress tensors are

$$\mathbf{E}_m = \frac{1}{2ka^2} U^s \epsilon_c \mathbf{G}_S^W, \tag{132}$$

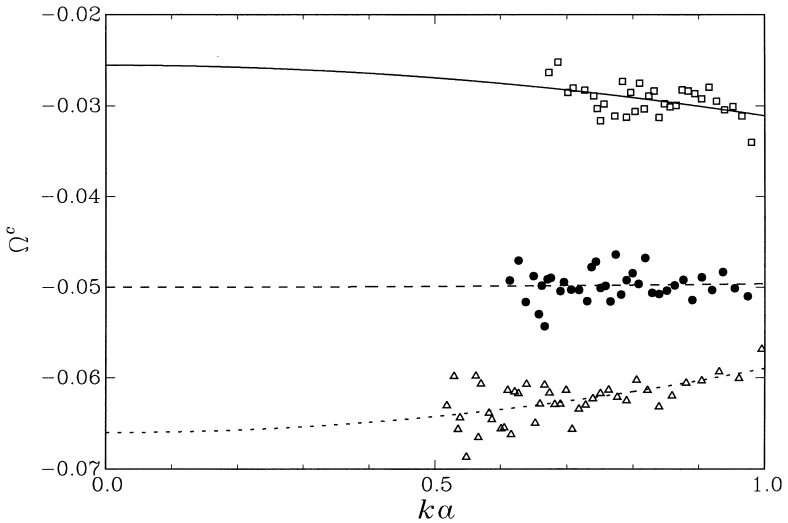


Fig. 16. The coefficient $\Omega^c$ defined in Eq. (130) as a function of $ka$ for $\beta_D^0 = 15\%$ (triangles), 25% (bullets), and 35% (squares). The lines are least-squares fits of the form (117).

$$\frac{1}{\mu_C}\boldsymbol{\Sigma}_P + 2\mathbf{E}_m = \frac{1}{ka^2}\left(\frac{9}{2}\beta^s - \ell_A^c\right)\mathbf{G}_S^W\epsilon_c + \frac{1}{ka^2}\left(\ell_A^c\mathbf{G}_A^W + \ell_M^c\mathbf{G}_M^W + \ell_I^c\mathbf{G}_I^W\right)\epsilon_c. \tag{133}$$

The first term in the right-hand side of this relation is proportional to $2\mathbf{E}_m$ and therefore defines the effective viscosity of the suspension:

$$\frac{\mu_{\text{eff}}}{\mu_C} = \lim_{ka\to 0}\frac{\frac{9}{2}\beta^s - \ell_A^c}{U^s}. \tag{134}$$

The results given by this formula are shown by the circles in Fig. 6, where they are seen to be in excellent agreement with the solid line which represents the effective viscosity calculated in the usual way by studying a homogeneous suspension subject to simple shear as described in the next section.

## 9. Results: simple shear

As remarked at the end of Section 6, for a uniform particle distribution (for which $\epsilon = 0$), the mixture possesses a stress–strain relation of the Newtonian type with an effective viscosity that can readily be written down upon comparing Eqs. (78) and (79):

$$\frac{\mu_{\text{eff}}}{\mu_C} = 1 + \frac{1}{2}\ell^0. \tag{135}$$

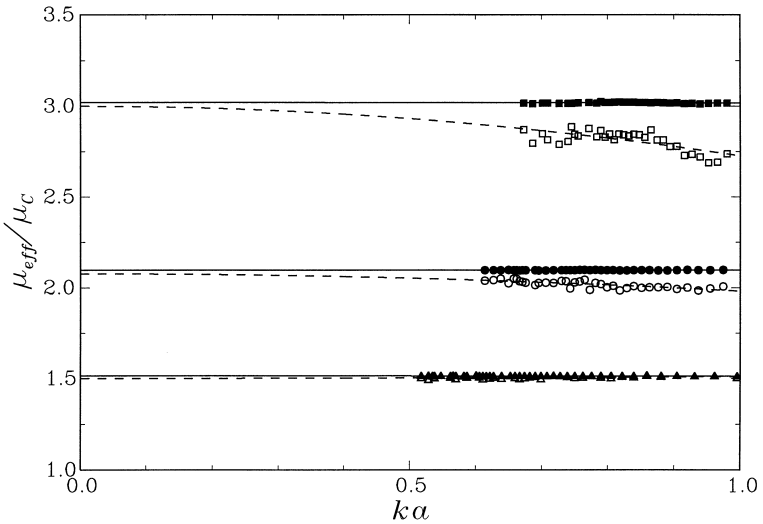


Fig. 17. The black symbols are the numerical results for the effective viscosity as defined in Eq. (135). Triangles are for $\beta_D^0 = 15\%$, circles for $\beta_D^0 = 25\%$, and squares for $\beta_D^0 = 35\%$. The solid lines are least-squares fits that reduce to a constant in this case. The open symbols are the right-hand side of Eq. (160) before taking the limit $ka\to 0$. The dashed lines are least-squares fits of form the (117).

It can be shown analytically that this result coincides with the expression for the same quantity given, e.g. by Batchelor (1970) and Mo and Sangani (1994).

This quantity, as calculated in the present simulations, is shown by the black symbols and the solid lines as a function of $ka$ for different $\beta_D^0$ in Fig. 17 (the dashed lines will be discussed in the next section). The solid lines are least-squares quadratic fits which simply reduce to constants showing that the result is independent of $ka$. The values of these constants, shown as function of $\beta_D^0$ in Fig. 6 (triangles), have been fitted to an expression of the form (109) to generate the solid line in this figure. These results have been obtained with five singularities per particle and differ from those of Mo and Sangani (1994) by about 4%. We have done the same simulations in a limited number of cases with 6 singularities finding a difference of only 1%.

Nunan and Keller (1984) have shown that, in a lattice, viscosity is a tensor given by an isotropic part plus a non-isotropic term proportional to a single constant. We have verified that the non-isotropic part of our result decreased below 6% already for 25 particles in the cell, and was less than 2% with more than 40 particles. These observations strengthen the conclusions of Section 7 on the small effects of the artificial periodicity and cell-side directions imposed by the present cell simulations. As in the previous case, we also find $Q^0 = 0$, so that $p_m = \langle pc \rangle = \overline{p^e}$ for a uniform suspension.

Turning now to the non-uniform case, the numerical results indicate that all the coefficients $\ell$ with superscript $c$ vanish, and also $w_{\parallel}^s = w_{\perp}^s = 0$. The situation is thus in some sense the reciprocal of the one encountered in the case of sedimentation where all the $\ell^s$ coefficients and $w_{\parallel}^c$, $w_{\perp}^c$ vanished. The expression for $\mathbf{u}_m$ becomes

$$\mathbf{u}_m - \mathbf{U}_\infty = \frac{1}{k}\mathbf{U}^c \epsilon_c \boldsymbol{\gamma}^\perp, \tag{136}$$

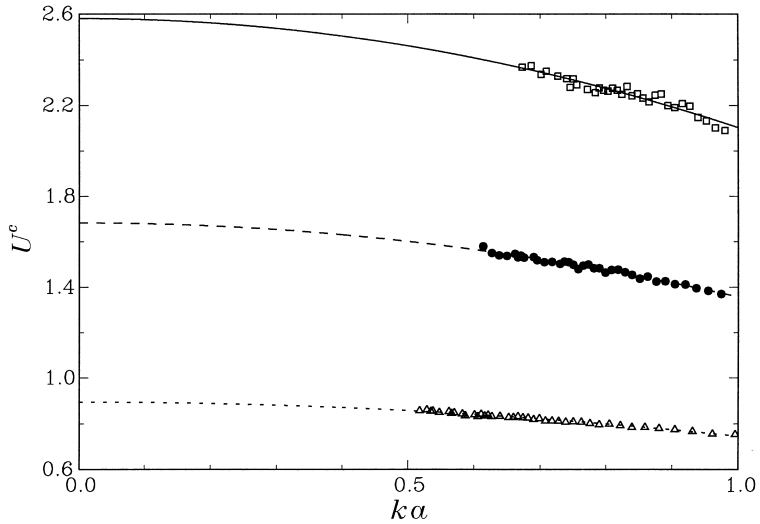


Fig. 18. Coefficient $U^c$ in Eq. (136) as a function of $ka$ for $\beta_D^0 = 15\%$ (triangles), 25% (bullets), and 35% (squares). The lines are least-squares fits of the form (117).

where

$$U^c = \frac{1}{ka}\left(\ell_S^s + \ell_A^s + \ell_\gamma^s\right) \tag{137}$$

which shows that $\mathbf{u}_m \neq \mathbf{U}_\infty$ only when the inhomogeneity is perpendicular to $\boldsymbol{\gamma}\cdot\mathbf{m}$; $U^c$, shown in Fig. 18, tends to a nonzero constant as $ka \to 0$. The corresponding expression for $\bar{\mathbf{w}}$ is

$$\bar{\mathbf{w}} - U_\infty = \frac{1}{k^2 a}\left(w_\perp^c \boldsymbol{\gamma}^\perp + w_\parallel^c \boldsymbol{\gamma}^\parallel\right)\epsilon_c, \tag{138}$$

with which we have the following expression for the slip velocity

$$\mathbf{u}_\Delta = ka^2\left(u_\perp^c \boldsymbol{\gamma}^\perp + u_\parallel^c \boldsymbol{\gamma}^\parallel\right)\epsilon_c, \tag{139}$$

where

$$u_\perp^c = \frac{1}{k^2 a^2}\left(\frac{w_\perp^c}{ka} - U^c\right), \qquad u_\parallel^c = \frac{1}{k^3 a^3} w_\parallel^c. \tag{140}$$

The coefficients $u_\perp^c$ and $u_\parallel^c$ are shown in Figs. 19 and 20. In spite of the numerical noise, these results indicate a non-zero, if small, interphase slip.

The expression for the mean pressure reduces to

$$\frac{1}{\mu_C} p_m = \frac{1}{ka} P^s \epsilon_s \left(\boldsymbol{\gamma}^\parallel \cdot \mathbf{m}\right), \tag{141}$$

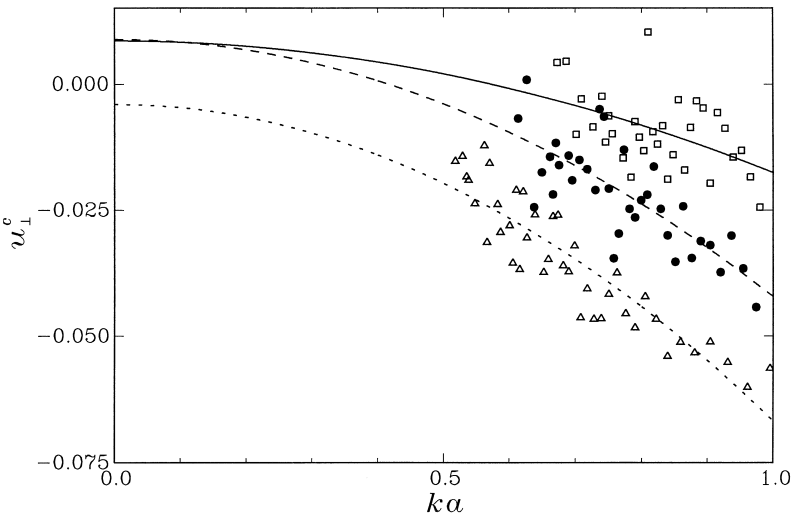


Fig. 19. Coefficient $u_\perp^c$ in Eq. (139) as a function of $ka$ for $\beta_D^0 = 15\%$ (triangles), 25% (bullets), and 35% (squares). The lines are least-squares fits of the form (117).

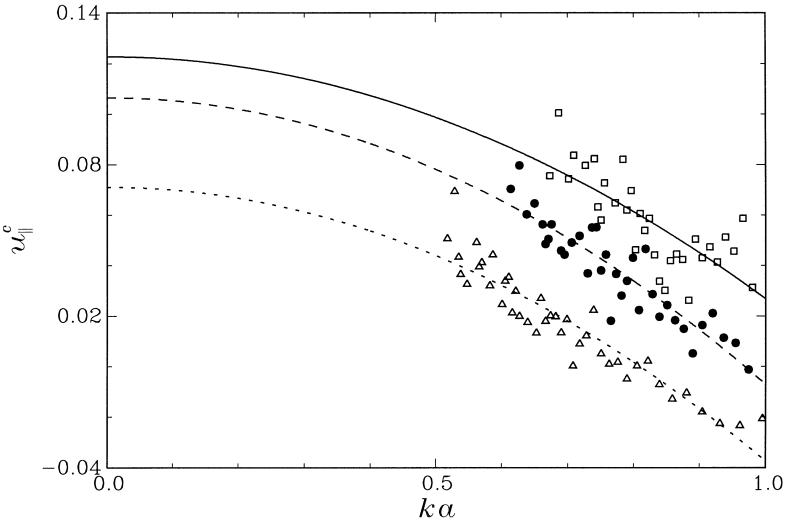


Fig. 20. Coefficient $u^c_\parallel$ in Eq. (139) as a function of $ka$ for $\beta^0_D = 15\%$ (triangles), 25% (bullets), and 35% (squares). The lines are least-squares fits of the form (117).

while

$$\frac{1}{\mu_C}\langle p_C\rangle = \frac{1}{ka} q^s \epsilon_s \left(\boldsymbol{\gamma}^{\parallel} \cdot \mathbf{m}\right), \tag{142}$$

from which $\zeta_p$ defined by Eq. (124) is

$$\zeta_p = \frac{q^s}{P^s}. \tag{143}$$

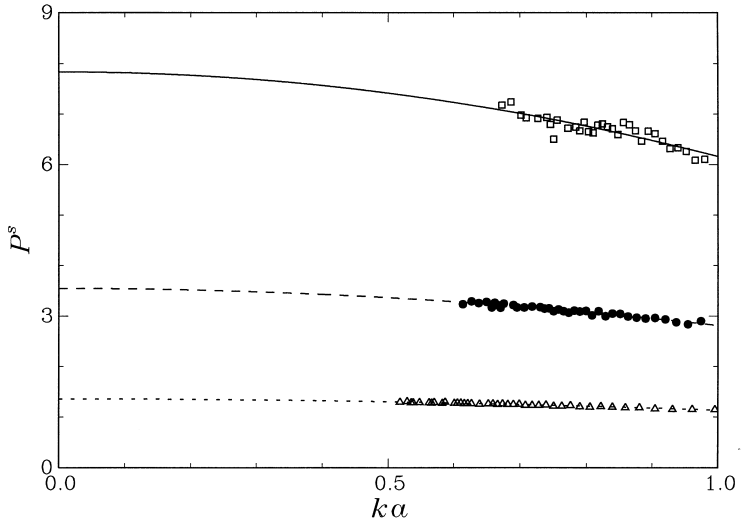


Fig. 21. The coefficient $P^s$ in Eq. (141) as a function of $ka$ for $\beta^0_D = 15\%$ (triangles), 25% (bullets), and 35% (squares). The lines are least-squares fits of the form (117).

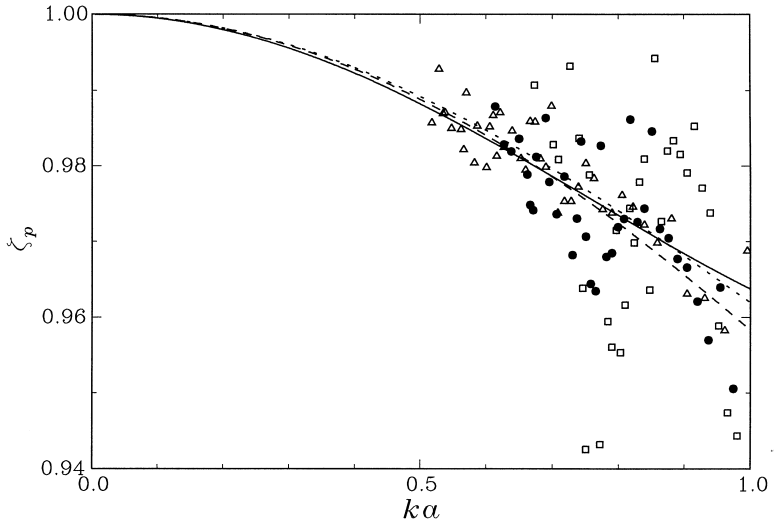


Fig. 22. The coefficient $\zeta_p$ defined in Eq. (143) for the simple shear case as a function of $ka$ for $\beta_D^0 = 15\%$ (triangles), 25% (bullets), and 35% (squares). The lines are biquadratic least-squares fits subject to the condition that $\zeta_p = 1$ at $ka = 0$.

The quantities $P^s$ and $\zeta_p$ are graphed in Figs. 21 and 22; $\zeta_p$ is fitted as $1 + \delta(ka)^2 + \zeta(ka)^4$ on the basis of the same argument outlined after Eq. (125) for the sedimentation case. Note that the scatter appears large chiefly because of the small range of the vertical scale.

The mean angular velocity of the particles and the vorticity of the suspending fluid are both zero for a uniform suspension, but not for a non-uniform one. We find $\omega^c = 0$ and, therefore, we have a relation similar to Eq. (127) with

$$\zeta_\Omega = -\frac{2\omega^s}{U^c}. \tag{144}$$

This quantity is shown in Fig. 23 from which we see that indeed the fluid and solid particle angular velocities are equal in the limit $ka \to 0$. At finite $ka$, however, the rotation rate of the particles differs from that of the fluid when the suspension is not uniform. Because $\zeta_\Omega \to 1$ as $ka \to 0$, the slip angular velocity can be expressed as

$$\boldsymbol{\Omega}_\Delta = k^2 a^2 \Omega^s \epsilon_s \mathbf{m} \times \boldsymbol{\gamma}^\perp, \tag{145}$$

where

$$\Omega^s = \frac{1}{k^2 a^2}\left(\frac{\omega^s}{ka} + \frac{1}{2}U^c\right), \tag{146}$$

approaches a nonzero constant as $ka \to 0$ as shown in Fig. 24.

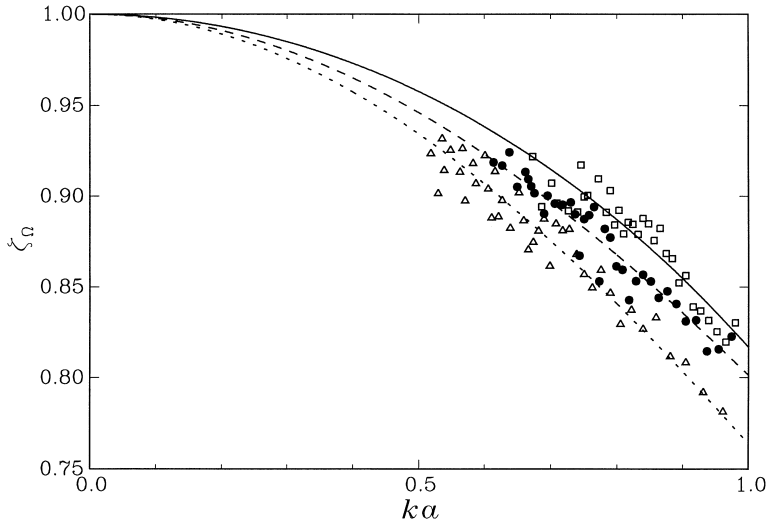


Fig. 23. The coefficient $\zeta_\Omega$ defined in (144) for the simple shear case as a function of $ka$ for $\beta_D^0 = 15\%$ (triangles), 25% (bullets), and 35% (squares). The lines are biquadratic least-squares fits subject to the condition that $\zeta_\Omega = 1$ at $ka = 0$

## 10. Results: couple

For a uniform suspension, the particles rotate with an average angular velocity proportional to the applied couple

$$\bar{\boldsymbol{\Omega}} - \boldsymbol{\Omega}_\infty = \Psi\left(\beta_D^0\right)\boldsymbol{\omega}, \tag{147}$$

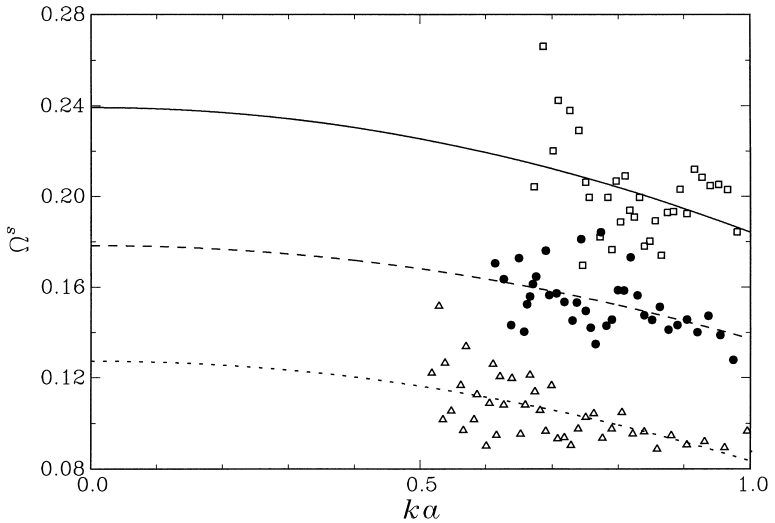


Fig. 24. The coefficient $\Omega^s$ defined in (146) as a function of $ka$ for $\beta_D^0 = 15\%$ (triangles), 25% (bullets), and 35% (squares). The lines are least-squares fits of the form (117)

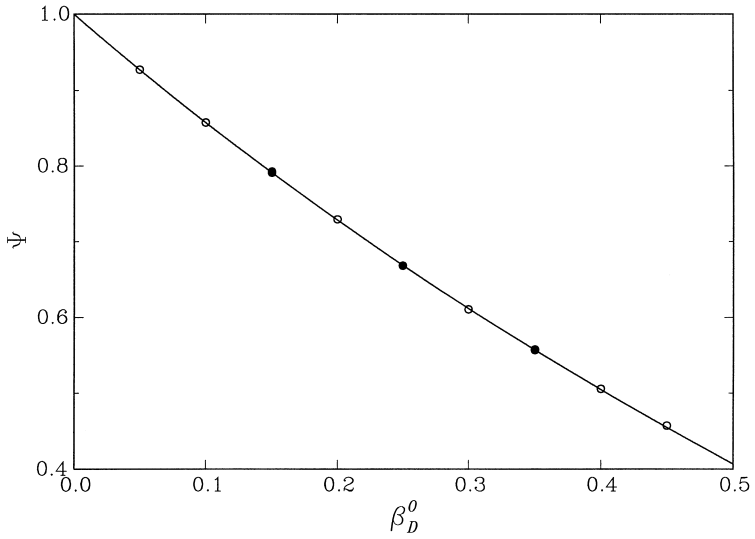


Fig. 25. Hindrance function for rotation, Eq. (147), as a function of $\beta_D^0$ for a uniform suspension. The black circles have been obtained on the basis of extensive simulations with variable number of particles and averages over thousands of configurations. The open circles have been obtained with only 28 particles per cell averaging over 500 configurations. The solid line is the fit (148).

where $\Psi(\beta_D^0)$ is the hindrance function for rotation (Brenner, 1970, 1972, 1984). A graph of this quantity is shown in Fig. 25; the numerical results are fitted by

$$\Psi\left(\beta_D^0\right) = \left(1-\beta_D^0\right)^{c_1-c_2\beta_D^0}, \tag{148}$$

where $c_1 = 1.50$, $c_2 = 0.41$. We find that $\Psi$ depends only very weakly, if at all, on $ka$.

Dropping quantities found numerically to vanish, the necessary formulae can be written as

$$\bar{\boldsymbol{\Omega}} - \boldsymbol{\Omega}_\infty = \Psi\left(\beta_D^0\right)\boldsymbol{\omega} + \frac{\omega_\parallel^s}{ka}\epsilon_s\boldsymbol{\omega}^\parallel + \frac{\omega_\perp^s}{ka}\epsilon_s\boldsymbol{\omega}^\perp \tag{149}$$

$$\mathbf{u}_m - \mathbf{U}_\infty = \frac{1}{k}U\epsilon_c(\mathbf{m}\times\boldsymbol{\omega}), \tag{150}$$

$$\bar{\mathbf{w}} - \mathbf{U}_\infty = \frac{w_\perp^c}{k^2a}\epsilon_c(\mathbf{m}\times\boldsymbol{\omega}), \tag{151}$$

$$p_m = \overline{p^e} = \langle p_C\rangle = 0, \tag{152}$$

with

$$U = \frac{1}{ka}\left(\ell_S^s + \ell_A^s\right). \tag{153}$$

The slip angular velocity is

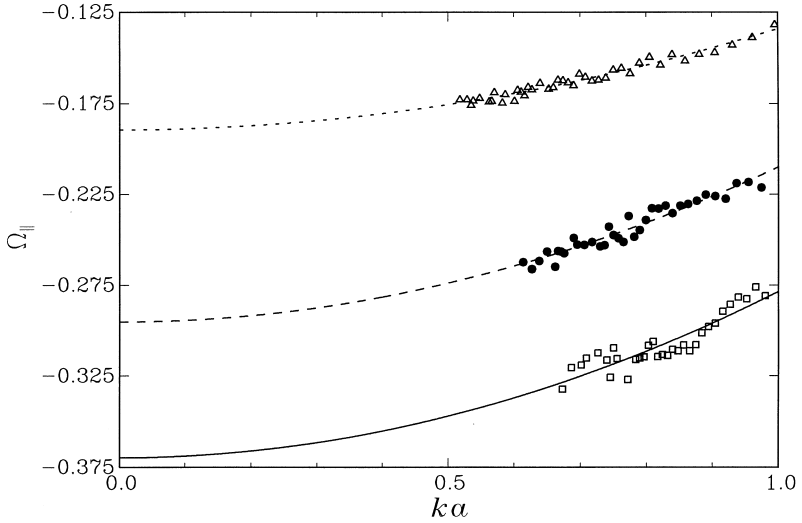


Fig. 26. The coefficient $\Omega_{\parallel}$ in Eq. (154) as a function of $ka$ for $\beta_D^0 = 15\%$ (triangles), 25% (bullets), and 35% (squares). The lines are least-squares fits of the form (117)

$$\boldsymbol{\Omega}_{\Delta} = \Psi\left(\beta_D^0\right)\boldsymbol{\omega} + \left(\Omega_{\parallel}\boldsymbol{\omega}^{\parallel} + \Omega_{\perp}\boldsymbol{\omega}^{\perp}\right)\epsilon_s \tag{154}$$

where

$$\Omega_{\parallel} = \frac{1}{ka}\omega_{\parallel}^s, \qquad \Omega_{\perp} = \frac{\omega_{\perp}^s}{ka} - \frac{1}{2}U. \tag{155}$$

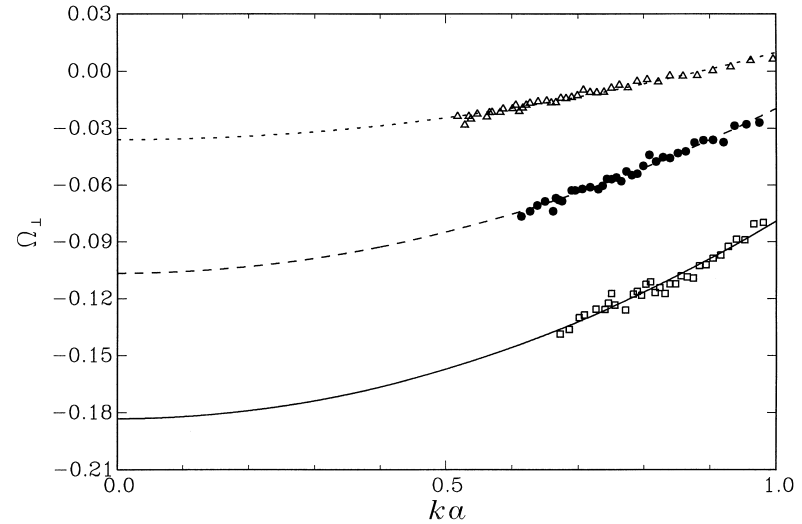


Fig. 27. The coefficient $\Omega_{\perp}$ in Eq. (154) as a function of $ka$ for $\beta_D^0 = 15\%$ (triangles), 25% (bullets), and 35% (squares). The lines are least-squares fits of the form (117)

Figs. 26 and 27 show $\Omega_{\parallel}$ and $\Omega_{\perp}$ together with least squares fits of the form (117). It is interesting to note that, whenever $\mathbf{m}\cdot\boldsymbol{\omega}\neq 0$, the average particle angular velocity is not parallel to the local vorticity $\frac{1}{2}\nabla\times\mathbf{u}_m-\boldsymbol{\Omega}_\infty$.

The slip velocity is given by

$$\mathbf{u}_\Delta = ka^2 u\epsilon_c(\mathbf{m}\times\boldsymbol{\omega}), \tag{156}$$

where

$$u=\frac{1}{k^2a^2}\left(\frac{w_\perp^c}{ka}-U\right), \tag{157}$$

which is shown in Fig. 28; the lines are quadratic fits of the form (117).

The strain rate is

$$\mathbf{E}_m=-\frac{1}{2}U\epsilon_s\mathbf{G}_S^\omega, \tag{158}$$

while, for the stress, we have

$$\frac{1}{\mu_C}\boldsymbol{\Sigma}_P+2\mathbf{E}_m=-\frac{1}{ka}\ell_A^s\epsilon_s\mathbf{G}_S^\omega+\frac{1}{ka}\ell_A^s\epsilon_s\mathbf{G}_A^\omega. \tag{159}$$

As in Section 8, we then find the following expression for the effective mixture viscosity:

$$\frac{\mu_{\text{eff}}}{\mu_C}=\lim_{ka\to 0}\frac{\ell_A^s}{kaU}. \tag{160}$$

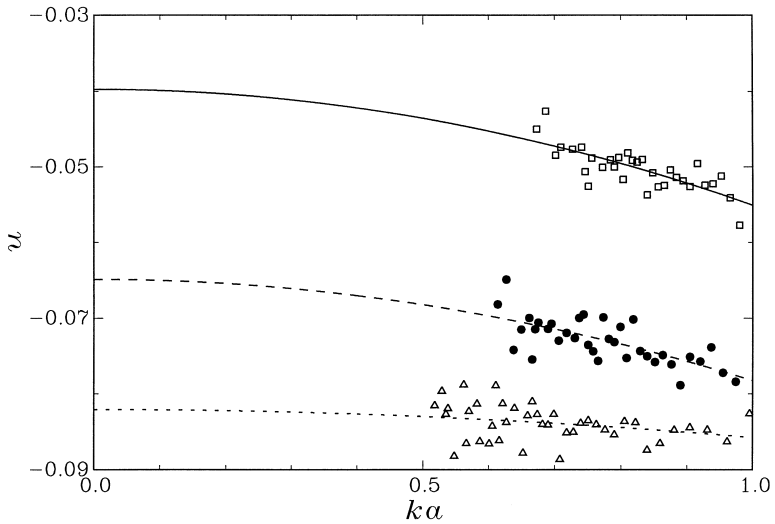


Fig. 28. The coefficient $u$ in Eq. (156) as a function of $ka$ for $\beta_D^0=15\%$ (triangles), 25% (bullets), and 35% (squares). The lines are least-squares fits of the form (117)

The numerical results for $\ell_A^s/kaU$ are shown by the open symbols and dashed lines in Fig. 17 as functions of $ka$. Note how close the limit values for $ka \to 0$ are to those found for the simple shear case in the previous section. These limit values correspond to the effective viscosity for the present case and are shown by the diamonds in Fig. 6, where this agreement is confirmed.

## 11. Conclusions

The purpose of this paper is to describe a method for the numerical ensemble averaging of flow quantities for particular flows of spatially non-uniform suspensions and to present results illustrating the behavior of such systems. In Part II of this study, we shall build on these results to derive in a systematic way constitutive relations that enable us to formulate averaged equations models to describe such flows.

Our results show that non-uniform suspensions behave very differently from uniform ones. Among the principal results, we mention the following:

1. A method has been devised to calculate the effective viscosity of suspensions for the cases of settling and rotation, in addition to the case of simple shear considered by earlier investigators. Such a calculation can be carried out for settling and rotation only for a non-uniform suspension. All three calculations give consistent results, which proves that the concept of effective viscosity is a robust one, most likely independent of the particular nature of the flow.
2. While the stress tensor in a uniform suspension can be reduced to a Newtonian form with an effective viscosity, this is not possible in the non-uniform case. The rheological behavior of a non-uniform suspension is much more complex. A closure relation will be given in Part II.
3. We have encountered cases in which the particle-mixture relative velocity does not vanish in spite of the absence of external forces on the particles. Such results have obvious implications for the well-known — and much debated — phenomenon of shear-induced particle migration (see e.g. Leighton and Acrivos, 1987; Acrivos, 1995).
4. The average pressure field in a suspension cannot be taken to equal the average continuous-phase pressure. The near-field disturbance induced by the particles plays an essential role in establishing the effective mixture pressure.
5. The settling or shearing of a non-uniform suspension causes a non-zero particle rotation that contributes to the stress.

These results have been obtained assuming that the particles are randomly distributed hard spheres. This is certainly a limitation as the particle distribution in a flowing suspension is known to depend on the flow. Nevertheless these are the first results which specifically show the major qualitative aspects in which a non-uniform suspension differs from a uniform one and one may expect that qualitatively similar differences would exist also for a more realistic particle distribution function.

**Acknowledgements**

The authors express their gratitude to Prof. A. Sangani for supplying the original code on which the one used in this study was based. The support by NSF and DOE under grants CTS-9521373 and DE-FG02-89ER14043, respectively, is gratefully acknowledged.

## Appendix A. The dilute limit

Zhang and Prosperetti (1997) derive three momentum equations in the dilute limit: one for the continuous phase,

$$0 = -\beta_C \nabla \langle p_C \rangle + \beta_C \rho_C \mathbf{g} + \beta_C \nabla \cdot \left[ 2\mu_C \left( 1 + \frac{5}{2}\beta_D \right) \mathbf{E}_m \right]$$

$$+ \frac{9\beta_D \mu_C}{2a^2} (\bar{\mathbf{w}} - \langle \mathbf{u}_C \rangle) - \frac{3}{4}\beta_D \mu_C \nabla^2 \langle \mathbf{u}_C \rangle$$

$$+ \frac{3}{4}\mu_C \nabla^2 \left[ \beta_D (\bar{\mathbf{w}} - \langle \mathbf{u}_C \rangle) \right] + 3\mu_C \nabla \times \left[ \beta_D \left( \bar{\boldsymbol{\Omega}} - \frac{1}{2} \nabla \times \langle \mathbf{u}_C \rangle \right) \right], \tag{A1}$$

one for the linear momentum of the disperse phase,

$$0 = -\beta_D \nabla \langle p_C \rangle + 2\mu_C \beta_D \nabla \cdot \mathbf{E}_C - \frac{9\mu_C \beta_D}{2a^2} (\bar{\mathbf{w}} - \langle \mathbf{u}_C \rangle) + \frac{3}{4}\mu_C \beta_D \nabla^2 \langle \mathbf{u}_C \rangle + \beta_D \rho_D \mathbf{g}, \tag{A2}$$

and one for the angular momentum of the disperse phase,

$$0 = 6\beta_D \mu_C \left( \frac{1}{2} \nabla \times \langle \mathbf{u}_C \rangle - \bar{\boldsymbol{\Omega}} \right) + n\mathbf{T} \tag{A3}$$

To express these momentum equations in terms of quantities used in the present paper, we need two other relations from Zhang and Prosperetti (1997):

$$\mathbf{u}_m = \beta_C \langle \mathbf{u}_C \rangle + \beta_D \langle \mathbf{u}_D \rangle \approx \beta_C \langle \mathbf{u}_C \rangle + \beta_D \bar{\mathbf{w}}, \tag{A4}$$

and

$$\mathbf{E}_m = \mathbf{E}_C + \mathrm{Symm}\left( \nabla \left[ \beta_D (\bar{\mathbf{w}} - \langle \mathbf{u}_C \rangle) \right] \right). \tag{A5}$$

Note that the dilute-limit equations in the form presented here are accurate to order $k^0$ for the sedimentation problem and to order $k$ for the shear and couple problems. Note also that Zhang and Prosperetti (1997) did not incorporate the body force on the continuous phase into a modified pressure, as is done in the present paper. Adding the second and third equations to the first one, and dropping terms of higher order in $\beta_D$ and $k$, we obtain the following three equations:

$$0 = -\frac{1}{\mu_C}\nabla\langle p_C\rangle + \beta_D\frac{2a^2}{9}\mathbf{W} + \nabla\cdot\left[2\left(1+\frac{5}{2}\beta_D\right)\mathbf{E}_m\right] + \frac{3}{4}\nabla^2\left(\beta_D\mathbf{u}_\Delta\right) + 3\nabla\times\left(\beta_D\boldsymbol{\omega}\right), \tag{A6}$$

$$\beta_D\mathbf{W} = \beta_D\left(\mathbf{u}_\Delta - \frac{a^2}{6}\nabla^2\mathbf{u}_m\right), \tag{A7}$$

and

$$\beta_D\boldsymbol{\omega} = \beta_D\bar{\boldsymbol{\Omega}}_\Delta. \tag{A8}$$

The solution to these equations is readily found in the three cases of sedimentation, simple shear, and applied couple. In order to treat all three cases together, as in Sections 8–10, we set

$$\beta_D = \beta_D^0 + \beta_D^s\epsilon_s \tag{A9}$$

$$\frac{1}{\mu_C}\langle p_C\rangle = \frac{9}{2a^2}p^0\mathbf{W}\cdot\mathbf{x} + \frac{p_W}{ka^2}\epsilon_c\mathbf{W}^\parallel\cdot\mathbf{m} + \frac{p_\gamma}{a}\epsilon_s\boldsymbol{\gamma}^\parallel\cdot\mathbf{m} \tag{A10}$$

$$\mathbf{u}_m = \boldsymbol{\gamma}\cdot\mathbf{x} + \frac{U^s}{k^2a^2}\epsilon_s\mathbf{W}^\perp + \frac{U^c}{k}\epsilon_c\boldsymbol{\gamma}^\perp + \frac{U}{k}\epsilon_c\mathbf{m}\times\boldsymbol{\omega} \tag{A11}$$

$$\mathbf{u}_\Delta = u^0\mathbf{W} + \left(u_\parallel^s\mathbf{W}^\parallel + u_\perp^s\mathbf{W}^\perp\right)\epsilon_s + ka^2\left(u_\parallel^c\boldsymbol{\gamma}^\parallel + u_\perp^c\boldsymbol{\gamma}^\perp\right)\epsilon_c + ka^2u\mathbf{m}\times\boldsymbol{\omega}\epsilon_c \tag{A12}$$

$$\bar{\boldsymbol{\Omega}}_\Delta = \Omega^0\boldsymbol{\omega} + k\Omega^c\epsilon_c\mathbf{m}\times\mathbf{W}^\perp + k^2a^2\Omega^s\epsilon_s\mathbf{m}\times\boldsymbol{\gamma}^\perp + \left(\Omega_\parallel\boldsymbol{\omega}^\parallel + \Omega_\perp\boldsymbol{\omega}^\perp\right)\epsilon_s \tag{A13}$$

We substitute these relations into the momentum equations and solve for the coefficients. All quantities not given explicitly are equal to zero.

Sedimentation ($\boldsymbol{\gamma} = \mathbf{T} = 0$),

$$p^0 = \beta_C^0\rho_C + \beta_D^0\rho_D, \quad p_W = -\frac{9\beta_D^s}{2}\left(1-\frac{a^2k^2}{6}\right), \qquad U^s = \frac{9\beta_D^s}{2}\left(1-\frac{a^2k^2}{6}\right), \tag{A14}$$

$$u^0 = 1 + O\left(\beta_D\right), \quad u_\parallel^s = u_\perp^s = \Omega^c = O\left(\beta_D\right). \tag{A15}$$

Simple shear ($\mathbf{g} = \mathbf{T} = 0$),

$$p_\gamma = 5\beta_D^s, \qquad U_c = 5\beta_D^s. \tag{A16}$$

$$u_\parallel^c = u_\perp^c = \Omega^s = O\left(\beta_D\right). \tag{A17}$$

Applied couple ($g = \boldsymbol{\gamma} = 0$),

$$U = 3\beta_D^s, \qquad \Omega^0 = 1 + O\left(\beta_D\right), \tag{A18}$$

$$u = \Omega_\parallel = O\left(\beta_D\right)\Omega_\perp = O\left(\beta_D\right). \tag{A19}$$

## References


Acrivos, A., 1995. Shear-induced particle diffusion in concentrated suspensions of non-colloidal particles. J. Rheol 39, 813–826.

Acrivos, A., Hinch, E.J., Jeffrey, D.J., 1980. Heat transfer to a slowly moving fluid from a dilute fixed bed of heated spheres. J. Fluid Mech 101, 403–421.

Allen, M.P., Tildesley, D.J., 1987. Computer Simulation of Liquids. Clarendon Press, Oxford.

Balucani, U., Zoppi, M., 1994. Dynamics of the Liquid State. Clarendon Press, Oxford.

Barnes, H.A., Hutton, J.F., Walters, K., 1990. An Introduction to Rheology. Elsevier, Amsterdam.

Batchelor, G.K., 1970. The stress system in a suspension of force-free particles. J. Fluid Mech 41, 545–570.

Batchelor, G.K., 1972. Sedimentation in a dilute dispersion of spheres. J. Fluid Mech 52, 245–268.

Batchelor, G.K., Green, J.T., 1972. The determination of the bulk stress in a suspension of spherical particles to order $c^2$. J. Fluid Mech 56, 401–427.

Biesheuvel, A., Spoelstra, S., 1989. The added mass coefficient of a dispersion of spherical gas bubbles in liquid. Int. J. Multiphase Flow 15, 911–924.

Bonnecaze, R.T., Brady, J.F., 1991. The effective conductivity of random suspensions of spheres. Proc. Roy. Soc. Lond A432, 445–465.

Brady, J.F., Bossis, G., 1988. Stokesian dynamics. Ann. Rev. Fluid Mech 20, 111–157.

Brady, J.F., Morris, J.F., 1997. Microstructure of strongly sheared suspensions and its impact on rheology and diffusion. J. Fluid Mech 348, 103–139.

Brenner, H., 1970. Rheology of a dilute suspension of dipolar spherical particles in an external field. J. Colloid Interface Sci 32, 141–158.

Brenner, H., 1972. Suspension rheology in the presence of rotary Brownian motion and external couples: elongational flow of dilute suspensions. Chem. Eng. Sci 27, 1069–1107.

Brenner, H., 1984. Antisymmetric stress induced by the rigid-body rotation of dipolar suspensions. Int. J. Engng. Sci 22, 645–682.

Buyevich, Yu.A., 1995. Interphase interaction in fine suspension flow. Chem. Eng. Sci 50, 641–650.

Buyevich, Yu.A., Ustinov, V.A., 1995. Effective thermal conductivity of a microscopically inhomogeneous dispersion. Int. J. Heat Mass Transfer 38, 381–389.

Cercignani, C., 1988. The Boltzmann Equation and Its Applications. Springer, New York.

Chang, C.Y., Powell, R.L., 1994a. The rheology of bimodal hard-sphere dispersions. Phys. Fluids 6, 1628–1636.

Chang, C.Y., Powell, R.L., 1994b. Self-diffusion of bimodal suspensions of hydrodynamically interacting spherical particles in shearing flow. J. Fluid Mech 281, 51–80.

Chapman, S., Cowling, T.G., 1952. The Mathematical Theory of Non-Uniform Gases, 3rd ed. Cambridge University Press, Cambridge, UK.

Cichocki, B., Felderhof, B.U., Hinsen, K., Wajnryb, E., Blawzdziewicz, J., 1994. Friction and mobility of many spheres in Stokes flow. J. Chem. Phys 100, 3780–3790.

Davis, R.H., Acrivos, A., 1985. Sedimentation of non-colloidal particles at low Reynolds numbers. Ann. Rev. Fluid Mech 17, 91–118.

Drew, D.A., 1983. Mathematical modeling of two-phase flow. Ann. Rev. Fluid Mech 15, 261–291.

Esmaeeli, A., Tryggvason, G., 1996. An inverse energy cascade in two-dimensional low Reynolds number bubbly flows. J. Fluid Mech. 315–330.

Feng, J., Hu, H.H., Joseph, D.D., 1994. Direct simulation of initial value problems for the motion of solid bodies in a Newtonian fluid, Part I: sedimentation. J. Fluid Mech 261, 95–134.

Feuillebois, F., 1984. Sedimentation in a dispersion with vertical inhomogeneities. J. Fluid Mech 139, 145–171.

Hansen, J.P., McDonald, I.R., 1990. Theory of Simple Liquids, 2nd ed. Academic Press, New York.

Hasimoto, H., 1959. On the periodic fundamental solutions of the stokes equations and their application to viscous flow past a cubic array of spheres. J. Fluid Mech 5, 317–328.

Hetsroni, G., 1982. Handbook of Multiphase Systems. Hemisphere, Washington DC.

Hinch, E.J., 1977. An averaged-equation approach to particle interactions in fluid suspension. J. Fluid Mech 83, 695–720.

Hu, H.H., 1996. Direct simulation of flows of solid–liquid mixtures. Int. J. Multiphase Flow 22, 335–352.

Ishii, M., 1975. Thermo-Fluid Dynamic Theory of Two-Phase Flow. Eyrolles, Paris.
Jeffrey, D.J., 1973. Conduction through a random suspension of spheres. Proc. R. Soc. Lond. A 335, 355–367.
Johnson, A.A., Tezduyar, T., 1996. Simulation of multiple spheres falling in a liquid-filled tube. Comp. Meth. Appl. Mech. Engng 134, 351–373.
Johnson, A.A., Tezduyar, T., 1997. 3-D simulation of fluid-particle interactions with the number of particles reaching 100. Comp. Meth. Appl. Mech. Engng 145, 301–321.
Jones, A.V., Prosperetti, A., 1985. On the suitability of first-order differential models for two-phase flow prediction. Int. J. Multiphase Flow 11, 133–148.
Kaftori, D., Hetsroni, G., Banerjee, S., 1995a. Particle behavior in the turbulent boundary layer. Part I: motion, deposition, and entrainment. Phys. Fluids 7, 1095–1106.
Kaftori, D., Hetsroni, G., Banerjee, S., 1995b. Particle behavior in the turbulent boundary layer. Part II: velocity and distribution profiles. Phys. Fluids 7, 1107–1121.
Ladd, A.J.C., 1988. Hydrodynamic interactions in a suspension of spherical particles. J. Chem. Phys 88, 5051–5063.
Ladd, A.J.C., 1990. Hydrodynamic transport coefficients of random dispersions of hard spheres. J. Chem. Phys 93, 3484–3494.
Ladd, A.J.C., 1993. Dynamical simulations of sedimenting spheres. Phys. Fluids 5, 299–310.
Ladd, A.J.C., 1997. Sedimentation of homogeneous suspensions of non-Brownian spheres. Phys. Fluids 9, 491–499.
Lamb, H., 1932. Hydrodynamics. Cambridge University Press, Cambridge, UK.
Landau, L., Lifshitz, E.M., 1969. Statistical Physics. Pergamon Press, Oxford.
Leighton, D., Acrivos, A., 1987. The shear-induced migration of particles in concentrated suspensions. J. Fluid Mech 181, 415–439.
Lhuillier, D., 1992. Ensemble averaging in slightly non-uniform suspensions. Eur. J. Mech. B/Fluids 11, 649–661.
Lhuillier, D., Nozières, P., 1992. Volume averaging of slightly non-homogeneous suspensions. Physica A181, 427–440.
Marchioro, M., Prosperetti, A., 1999. Conduction in non-uniform composites. Proc. Roy. Soc. Lond., A455, 1483–1508.
Marchioro, M., Tanksley, M., Prosperetti, A., 1999. Mixture pressure and stress in disperse two-phase flows. Int. J. Multiphase Flow, 25, 1395–1429.
Marchioro, M., Tanksley, M., Prosperetti, A., 2000. Flow of spatially non-uniform suspensions. Part II: Systematic derivation of closure relations. Int. J. Multiphase Flow, submitted.
Martys, N., Bentz, D.P., Garboczi, E.J., 1994. Computer simulation study of the effective viscosity in Brinkman's equation. Phys. Fluids 6, 1434–1439.
Mo, G., Sangani, A.S., 1994. A method for computing Stokes flow interactions among spherical objects and its application to suspensions of drops and porous particles. Phys. Fluids 6, 1637–1652.
Nott, P.R., Brady, J.F., 1994. Pressure-driven flow of suspensions: simulation and theory. J. Fluid Mech 275, 157–199.
Nunan, K.C., Keller, J.B., 1984. Effective viscosity of a periodic suspension. J. Fluid Mech 142, 269–287.
Pan, Y., Banerjee, S., 1996. Numerical simulation of particle interactions with wall turbulence. Phys. Fluids 8, 2733.
Phillips, R.J., Armstrong, R.C., Brown, R.A., 1992. A constitutive equation for concentrated suspensions that accounts for the shear-induced particle migration. Phys. Fluids A4, 30–40.
Prosperetti, A. 1998. Ensemble averaging techniques for disperse flows. In: Drew, D., Joseph, D.D., Passman, S.L. (Eds.), Particulate Flows: Processing and Rheology. Springer, Berlin, pp. 99–136.
Prosperetti, A., Jones, A.V., 1984. Pressure forces in disperse two-phase flows. Int. J. Multiphase Flow 10, 425–440.
Russell, W.B., Saville, D.A., Schowalter, W.R., 1989. Colloidal Dispersions. Cambridge University Press, Cambridge, UK.
Salacuse, J.J., Denton, A.R., Egelstaff, P.A., 1996. Finite-size effects in molecular dynamics simulations: Static structure factor and compressibility. Part I: theoretical method. Phys. Rev E53, 2382–2389.
Sangani, A.S., Acrivos, A., 1982. Slow flow through a periodic array of spheres. Int. J. Multiphase Flow 8, 343–360.
Sangani, A.S., Acrivos, A., 1983. The effective conductivity of a periodic array of spheres. Proc. Roy. Soc. Lond A386, 263–275.
Sangani, A.S., Mo, G.B., 1996. An $O(N)$ for Stokes and Laplace interactions of spheres. Phys. Fluids 8, 1990–2010.

Sangani, A.S., Mo, G.B., Tsao, H.K., Koch, D.L., 1996. Simple shear flow of dense gas–solid suspensions at finite Stokes numbers. J. Fluid Mech 313, 309–341.

Sangani, A.S., Yao, C., 1988. Bulk conductivity of composites with spherical inclusions. J. Appl. Phys 63, 1334–1341.

Stewart, H.B., Wendroff, B., 1984. Two-phase flows: models and methods. J. Comput. Phys 56, 363–409.

Studart, N., da Silveira, H.V., de Freitas, U., 1996. Effective field theory for hard-sphere fluids. Phys. Rev E53, 2350–2354.

Tanksley, M., Marchioro, M., Prosperetti, A., 1999. Average pressure and velocity fields in non-uniform suspensions of spheres in Stokes flow. J. Engng. Math., submitted.

Tezduyar, T.E., Mittal, S., 1994. Massively parallel finite element computation of incompressible flows involving fluid-body interactions. Comp. Meth. Appl. Mech. Eng 112, 253–282.

Throop, G.J., Bearman, R.J., 1965. Numerical solution of the Percus–Yevick equation for the hard-sphere potential. J. Chem. Phys 42, 2408–2411.

Torquato, S., 1987. Thermal conductivity of disordered heterogeneous media from the microstructure. Revs. Chem. Eng 4, 151–204.

Torquato, S., Lee, S.B., 1990. Computer simulations of nearest-neighbor distribution function and related quantities for hard-sphere systems. Physica A 167, 361–383.

Unverdi, S.O., Tryggvason, G., 1992. Computation of multi-fluid flows. Physica D 60, 70–83.

Weinbaum, S., Ganatos, P., Yan, Z.Y., 1990. Numerical multipole and boundary integral equation techniques in Stokes flow. Annu. Rev. Fluid Mech 22, 275–316.

Zhang, D.Z., Prosperetti, A., 1994a. Averaged equations for inviscid disperse two-phase flow. J. Fluid Mech 267, 185–219.

Zhang, D.Z., Prosperetti, A., 1994b. Ensemble phase-averaged equations for bubbly flows. Phys. Fluids 6, 2956–2970.

Zhang, D.Z., Prosperetti, A., 1997. Momentum and energy equations for disperse two-phase flows and their closure for dilute suspensions. Int. J. Multiphase Flow 23, 425–453.

Zuzovsky, M., Adler, P.M., Brenner, H., 1983. Spatially periodic suspensions of convex particles in linear shear flows. Part III: dilute arrays of spheres suspended in Newtonian fluids. Phys. Fluids 26, 1714–1723.